INVESTIGATION OF COPPER FOAM COLDPLATES AS A HIGH HEAT FLUX ELECTRONICS COOLING SOLUTION

A Thesis
Presented to
The Academic Faculty

By

Scott Wilson

In Partial Fulfillment
Of the Requirements for the Degree
Master of Science in Mechanical Engineering

Georgia Institute of Technology

May 2005

INVESTIGATION OF COPPER FOAM COLDPLATES AS A HIGH HEAT FLUX ELECTRONICS COOLING SOLUTION

Approved by:

Dr. Yogendra Joshi, Advisor
School of Mechanical Engineering
Georgia Institute of Technology

Dr. Andrei Fedorov
School of Mechanical Engineering
Georgia Institute of Technology

Dr. Samuel Graham
School of Mechanical Engineering
Georgia Institute of Technology

Date Approved: April 15, 2005

ACKNOWLEDGEMENT

I would like to thank Dr. Yogendra Joshi for his technical mentoring, direction, and support during this research. I would also like to thank Dr. Andrei Fedorov and Dr. Samuel Graham for their technical review and support as my thesis reading committee. I would like to thank my parents, David and Darlene Wilson, for their moral support during my graduate school experience. I extend my thanks to the fellow members of the Microelectronics and Emerging Technologies Thermal Laboratory, especially officemates Xiaojin Wei, Siva Gurrum, and Sunil Murthy. I thank my housemates, Adam Christensen, Matt Duff, and Dave Garth, for their camaraderie and encouragement. I thank all of my friends in Atlanta who have made my time in grad school a rich and fulfilling experience. I would like to thank Regina Neequaye for her administrative assistance and John Graham and the ME department machine shop staff for their assistance in machining the experimental hardware. I would like to thank K.C. Chou and the staff at S-Bond Inc. for their fabrication assistance. Finally, I would like to thank Delphi Corporation for the graduate fellowship and Foster-Miller, Inc. and the Office of Naval Research for the research funding.

TABLE OF CONTENTS

LIST OF TABLES

LIST OF FIGURES

LIST OF FIGURES

NOMENCLATURE

A_{cross}	Cross-sectional area of pore
c_p	Specific heat at constant pressure
D_h	Hydraulic diameter
d_p	Pore diameter
$k_{Coolant}$	Thermal conductivity of coolant
$k_{Faceplate}$	Thermal conductivity of faceplate
L	Thickness of unit cell
$L_{Faceplate\ thickness}$	Thickness of faceplate
$\dot{m}$	Mass flow rate
$N_{Unit\ cell}$	Total number of unit cells in direction of coolant flow
P	Wetted perimeter of pore
q”	Heat flux
$R_{Thermal}$	Thermal resistance of porous coldplate
Re	Reynolds number
$T(\vec{r})$	Temperature at inlet of first unit cell
$T(\vec{r}+\vec{L})$	Coolant temperature at exit of first unit cell and inlet of second unit cell
$T(\vec{r}+2\vec{L})$	Coolant temperature at exit of second unit cell
$T_{bulk,exit}$	Bulk coolant temperature at unit cell exit
$T_{bulk,inlet}$	Bulk coolant temperature at unit cell inlet
$T_{Coldplate\ Exit}$	Area-averaged coolant temperature at coldplate exit
$T_{Coldplate\ Inlet}$	Area-averaged coolant temperature at coldplate inlet
T_{Max}	Maximum coldplate faceplate temperature at trailing edge of foam

$T_{Unit\ cell\ exit}$	Area-averaged coolant temperature at exit face of unit cell
$T_{Unit\ cell\ foam\ top}$	Maximum interface temperature between the faceplate and the foam
U	Velocity of internal flow
λ	Thermal conductivity scaling factor
μ	Viscosity
ρ	Density
σ	Temperature gradient across periodic unit cell

SUMMARY

Compact heat exchangers such as porous foam coldplates have great potential as a high heat flux cooling solution for electronics due to their large surface area to volume ratio and tortuous coolant path. The focus of this work was the development of unit cell modeling techniques for predicting the performance of coldplates with porous foam in the coolant path.

Multiple computational fluid dynamics (CFD) models which predict porous foam coldplate pressure drop and heat transfer performance were constructed and compared to gain insight into how to best translate the foam microstructure into unit cell model geometry. Unit cell modeling in this study was realized by applying periodic boundary conditions to the coolant entrance and exit faces of a representative unit cell. A parametric study was also undertaken which evaluated dissimilar geometry translation recommendations from the literature. The use of an effective thermal conductivity for a representative orthogonal lattice of rectangular ligaments was compared to a porosity-matching technique of a similar lattice. Model accuracy was evaluated using experimental test data collected from a porous copper foam coldplate using deionized water as coolant. The compact heat exchanger testing facility which was designed and constructed for this investigation was shown to be capable of performing tests with coolant flow rates up to 300 mL/min and heat fluxes up to 290 W/cm^2. The greatest technical challenge of the testing facility design proved to be the method of applying the heat flux across a 1 cm^2 contact area. Based on the computational modeling results and experimental test data, porous foam modeling recommendations and porous foam coldplate design suggestions were generated.

CHAPTER 1

INTRODUCTION

Like the microprocessor industry, the power electronics industry must address thermal management issues to enable future devices to meet performance expectations. Cooling solutions are being sought for heat dissipation levels of up to 1000 W/cm^2 or higher as shown in Figure 1 [1] [2] [3] [4] [5] [6].

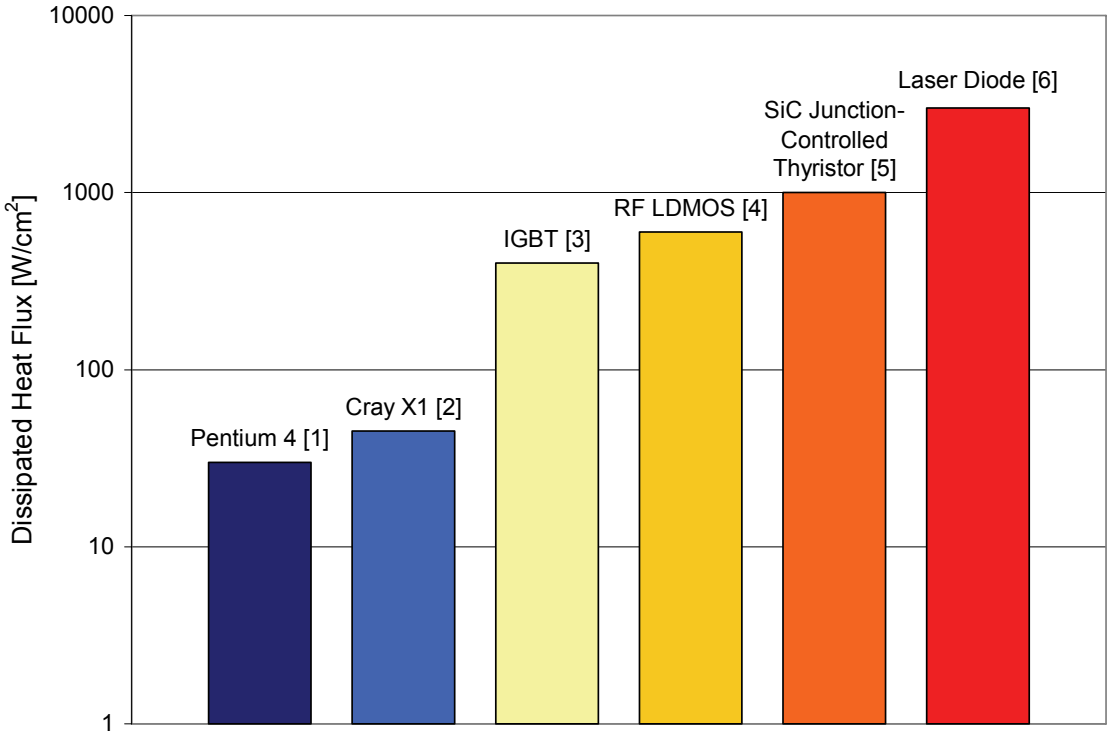

Figure 1: Power Electronics Heat Dissipation Levels

The issue of rising heat dissipation levels is impacting industries and research beyond power electronics such as laser mirrors [7] [8] [9], fusion power systems [10] [11] [12], high-power optical components [13], and high-power laser diode systems [14] [15]. Porous media such as metal foam are a leading candidate technology under exploration as a potential cooling solution for such applications. In this study, the cooling strategy of

embedding an open cell 100 pores per linear inch (ppi) Porvair copper foam element with 20% porosity within a copper coldplate for single-phase liquid cooling is evaluated computationally and experimentally. A cross-sectional view of such a coldplate, shown in Figure 2, includes a copper body, a faceplate, and a copper foam element. The copper foam element is fixed rigidly to the coldplate and is in direct contact with the 0.5 mm-thick faceplate.

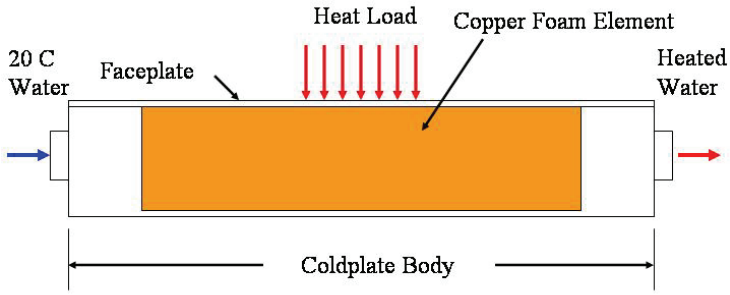

Figure 2: Cross-section of Porous Coldplate

Past recommendations from the literature are tested and compared to determine unit cell modeling techniques which can be implemented in predictive computational models to optimize the design of coldplates to address future electronics cooling concerns.

CHAPTER 2

LITERATURE REVIEW

Understanding the context of this research requires a review of past literature regarding the use of metal foams to enhance convective heat transfer and the history of predictive computational modeling of such phenomena. The promising results of past evaluations encourage further study of foam-filled coldplates

Research in fields such as optics and fusion energy has fueled the development and evaluation of foam-filled coldplates over the past 25 years. Soviet engineers and scientists began to make a tremendous contribution to this area in the late 1970s, led by Viktor Apollonov. Thermacore and Sandia National Laboratories have also invested in research in this area in the past decade. A summary of the past application studies can be found in Table 1. Difficulty arises in comparing such experimental work due to the differences in test duration, heat application area, and the lack of specific test details in the literature. In general, the applications studied in the literature often allow for a higher coldplate faceplate temperature than commercial power electronics components can withstand and focus on short duration test cases to measure the promise of the technology for such applications. Apollonov et al. allowed a coldplate faceplate, or substrate, temperature of 200°C [7]. Multiple test cases lasted 1 minute or less [11] [12]. Regardless of the specific test parameters, it can be said that foam-filled coldplates have been evaluated experimentally over the past 27 years for application in several industries.

Table 1: Application Studies of Convection Enhancement Via Metal Foam

Application	Year	Authors and Journal	Foam / Coolant	Heat Flux [kW/cm^2]	Details
Laser mirrors	1978	Apollonov et al. / Soviet Journal of Quantum Electronics [7]	Copper / Water	2.5	200°C substrate temperature
	1979	Apollonov et al. / Soviet Journal of Quantum Electronics [8]	Copper / Water	8	
	1980	Apollonov et al. / Optical Materials [9]	Copper / Water	4 to 5	
Fusion power systems	1991	Zapevalov et al. / Microwave Tube Journal [10]	N/A / Water	5	Reasonable flow rates and pressure drops
	1993	Rosenfeld et al. / High Heat Flux Engineering II [11]	Copper / Water	7.4	0.217 inch diameter heat application area, 20 s test duration
	1996	North et al. / High Heat Flux Engineering III [12]	Copper / Helium	4	1.6 cm^2 heat application area, 60 s test duration, 46.5°C inlet helium temperature
High-powered optical components	1995	Rosenfeld et al. / Optical Engineering [13]	Porous metal / Water	6	Flow rate of 0.023 L/s
High-power laser diode systems	1999	Apollonov et al. / Optics Express [14]	Porous metal / Water	0.92	
	2000	Apollonov et al. / Advanced High-Power Lasers [15]	Porous metal / Water	1	20°C inlet water temperature

The range of length scales involved and the random orientation of the foam ligaments cause the computational performance prediction of metal foam-filled coldplates to be challenging. Metal foam is an engineered material that is categorized as porous media. Darcy first considered flow through porous media in 1856 [16]. Since then, porous media research has developed more refined flow models and numerous heat transfer correlations for a myriad of scenarios. Much of the research can be broken down by physical structure into three groups: beds of spheres, bundles of rods, and foams. Table 2 contains an overview of important contributions to the field of metal foam modeling.

Table 2: Survey of Metal Foam Modeling Techniques

Modeling Technique	Year	Authors and Journal	Foam / Coolant	Details
Periodic unit cell	1980	Brenner / Phil. Trans. of Royal Soc. of London. Series A [17]	N/A	
Periodic unit cell	1989	Koch et al. / Journal of Fluid Mechanics [18]	N/A	
Bank of cylinders (BOC)	1997	Bastawros et al. / ASME EEP [19]	Aluminum foam / air	4-86 L/min air flow rate
Orthogonal lattice of ligaments	1998	Lu et al. / Acta Materialia [20]	N/A	
Effective thermal conductivity of a 3-D foam	2001	Boomsma et al. / Intl. Journal of Heat and Mass Transfer [21]	Aluminum foam / air and water	
Periodic unit of 8 cells, Porosity matching	2003	Boomsma et al. / Intl. Journal of Heat and Fluid Flow [22]	Open cell metal foam	Surface tension modeler created geometry; CFD-ACE by CFDRC is flow solver

CHAPTER 3

METHODOLOGY

3.1 Computational Modeling

Many modeling techniques exist for the analysis of porous foam. Three approaches were considered when formulating this study: the porous media model embedded in Fluent, the drag model for flow over a periodic array of vertical cylinders, and the three-dimensional unit cell model. Since the study sought to develop a predictive model without characterization of a physical specimen in advance, emphasis was placed on capturing the effect of the microstructure under evaluation through the chosen modeling approach. The three techniques considered for use in this study will be discussed in order of increasing foam microstructure modeling detail and are depicted in Figure 3.

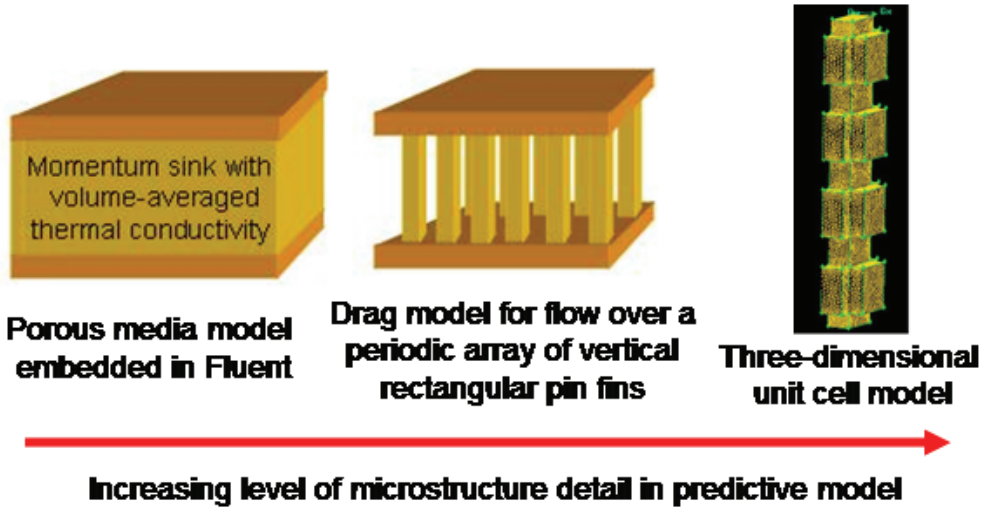

Figure 3: Modeling Technique Comparison

The Fluent porous media model employs a momentum equation which accounts for both viscous and inertial losses in the foam and includes an effective thermal conductivity in the energy equation calculated via volume-averaging the coolant and foam thermal

conductivities. The Fluent user's guide, Vafai et al., and Kaviany provide greater insight into this technique. [23] [24] [25] This approach was not followed because the Fluent formulation of the momentum equation requires user-defined empirical coefficients which were not available for the foam material utilized.

The drag model for flow over a periodic array of vertical cylinders is the intermediate technique on the spectrum of foam microstructure modeling techniques considered for this study. This approach accounts for the vertical foam ligaments shown in Figure 3 while ignoring the horizontal ligaments. Employed by Bastawros and Evans, this modeling technique simplifies the three-dimensional ligament structure into a vertical cylindrical pin fin array, a well-known geometry [19]. Since the heat load into the copper foam element comes only from the faceplate above, the vertical cylindrical pin fins would model well the heat conduction from the faceplate into the foam element, what Kharitonov et al. calls "the finning effect" [26]. The absence of the horizontal ligaments prevents accurate modeling of heat spreading between neighboring pin fins as it moves downward through the liquid-cooled foam. The heat transfer enhancement gained by the coolant-mixing flow over the horizontal ligaments would also be unaccounted for.

The three-dimensional unit cell model offers the highest level of foam microstructure resolution of the techniques considered. The unit cell is the smallest repeating pattern of the porous copper foam element which accurately captures the fluid dynamics and heat transfer of the entire element. Boomsma et al. also refer to a unit cell as a representative elementary volume (REV) [22]. This unit cell modeling technique allows the microstructure of porous foam to be modeled without the lengthy construction time and computational expense of modeling the entire metal foam element at the small ligament length scale. One of the earliest references to this technique was by Brenner in

1980 [17]. This technique is possible with the Fluent software package due to its ability to construct periodic boundary conditions on the upstream and downstream faces of the unit cell. The periodic boundary conditions imposed by Fluent treat the temperature change within the periodic unit cell according to equation (1) [23]:

$$\frac{T\left(\vec{r}+\vec{L}\right)-T\left(\vec{r}\right)}{L}=\frac{T\left(\vec{r}+2\vec{L}\right)-T\left(\vec{r}+\vec{L}\right)}{L}=\sigma \tag{1}$$

The temperature change can also be expressed in terms of the total heat added to the unit cell as in equation (2):

$$\sigma=\frac{Q}{\dot{m}c_p L}=\frac{T_{bulk,exit}-T_{bulk,inlet}}{L} \tag{2}$$

Similar periodic unit cells have been employed by Koch et al. and Boomsma et al. [18] [22]. The important assumptions of such a periodic unit cell model are:

1) the neglection of the interaction between the coolant and the two vertical side walls where the copper foam contacts the solid copper surfaces of the coldplate housing, shown in Figure 4
2) the assumption that all of the flow through the foam element is fully-developed along the direction of coolant flow, regardless of location perpendicular to the coolant flow

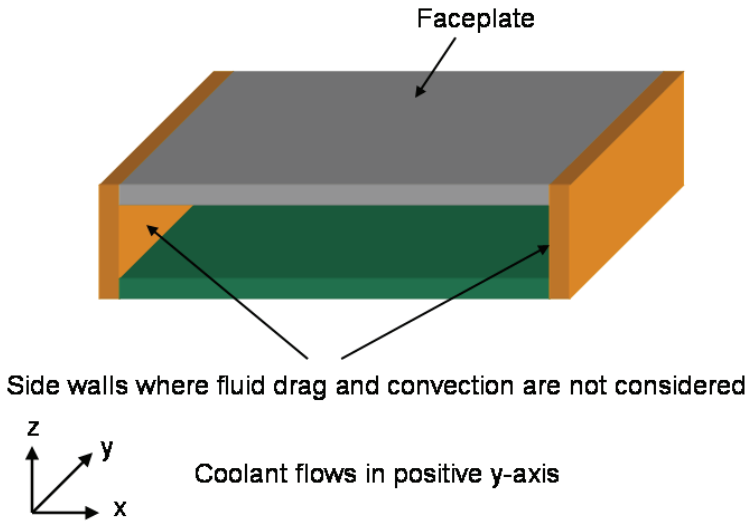

Figure 4: Diagram of Neglected Vertical Channel Walls

Given these assumptions, Fluent calculates the pressure drop across the unit cell and the temperature and coolant velocity fields throughout the unit cell including the exit face of the coolant region. The outlet temperature and velocity fields are then applied as entrance conditions for the second unit cell iteration. The model iterates, as shown in Figure 5, until a unit cell model is reached in which the solutions to the momentum and energy equations have converged.

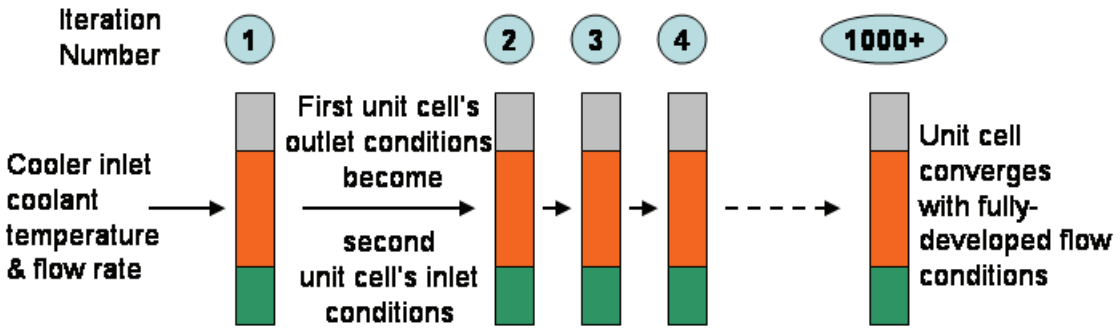

Figure 5: Unit Cell Convergence Process

Three predictive three-dimensional unit cell models were constructed in order to better understand the effects of the ligament diameter, porosity and effective thermal conductivity of the porous foam:

A. an open cell ligament model which matches the ligament diameter of the 100 ppi foam and is based on the work of Lu et al. [20]
B. an open cell ligament model based on the work of Boomsma et al. which matches the porosity of the model to the 20% porosity of the 100 ppi candidate foam [22]
C. an open cell model which is derived from scanning electron microscope images of the 100 ppi foam and which creates tortuous flow due to the non-orthogonality of the pore axes

Boomsma et al. [22] recommends determining the flow regime through open cell metal foam using the pore-based Reynolds number as listed in equation (3):

$$\mathrm{Re} = \frac{\rho U d_p}{\mu} \tag{3}$$

For the range of mass flow rates and geometries considered, the flow was calculated to be within the laminar regime as shown in Table 3. Radiation heat transfer within the porous coldplate is considered negligible in this investigation due to the relatively low surface temperatures and small temperature range between the surfaces involved.

Table 3: Flow Regime Calculations

Model	Flow Rate	Coolant Velocity	Pore Diameter	Pore-based Reynolds Number	Flow Regime
	[mL/min]	[m/s]	[m]	-	-
A	100	0.98	1.00E-04	97	Laminar
	200	1.90	1.00E-04	189	Laminar
	300	2.79	1.00E-04	277	Laminar
B	100	2.06	2.30E-05	47	Laminar
	200	4.17	2.30E-05	95	Laminar
	300	6.19	2.30E-05	141	Laminar
C	100	0.73	1.00E-04	72	Laminar
	200	1.43	1.00E-04	141	Laminar
	300	2.13	1.00E-04	211	Laminar

Ligament Diameter-Matching Model

A periodic unit cell model was constructed using Fluent computational fluid dynamics (CFD) software to predict the thermal and hydrodynamic performance of the coldplate based on the microstructure of the porous copper foam element. The CFD model proved computationally possible due to a unit cell approach to an open cell ligament model. The open cell ligament model presented by Lu et al. allows for the construction of a predictive model prior to empirical flow characterization of the porous foam element [20]. Such a design, shown in Figure 6, simplifies the microstructure by assuming orthogonal intersection of the foam ligaments. The model captures the conduction of heat through the vertical and horizontal copper ligaments, the convection of heat away from said ligaments, and the mixing effect of flow around them. The difference between the technique used here and the technique proposed by Lu et al. is that the ligament diameter in the model by Lu et al. is based on the relative foam density; whereas, the ligament diameter in this model is matched to the foam microstructure. The difference is motivated by the desire to develop a modeling technique which would require the simplest characterization of the candidate foam, such as ligament diameter

measurement. The orthogonal lattice of ligaments core to the proposal of Lu et al. is maintained. The porous copper foam element modeled is 1 cm x 1 cm x 0.1 cm with a 0.05 cm-thick faceplate on the top surface and a 0.05 cm-thick copper skin on the bottom surface, as shown in Figure 7. It is not necessary to model the rest of the coldplate body since the actual heat path is contained in this smaller domain of the coldplate. The periodic unit cell, also shown in Figure 6, is a second model size reduction. The ligament diameter-matching computational model consists of one unit cell, the geometry of which is shown in Figure 8.

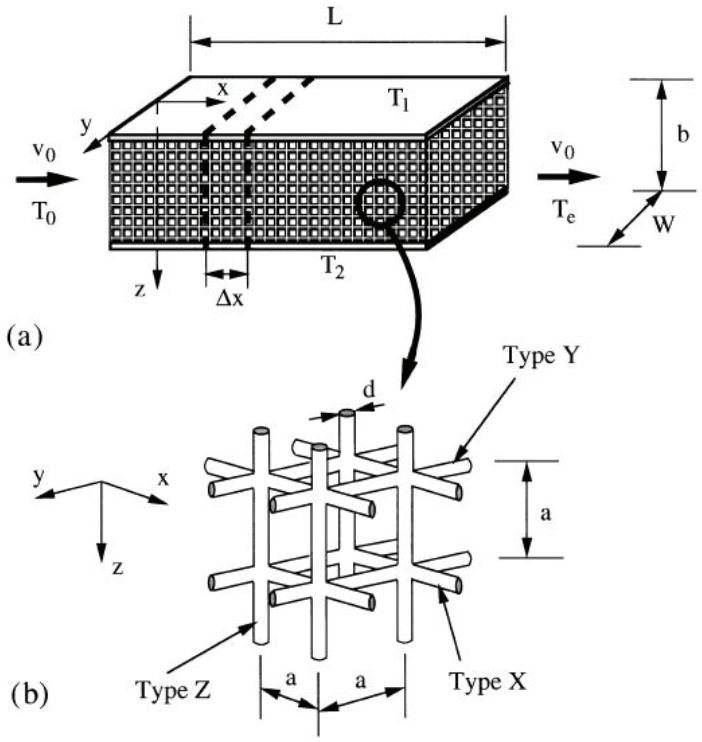

Figure 6: Ligament Model for Metal Foams [20]

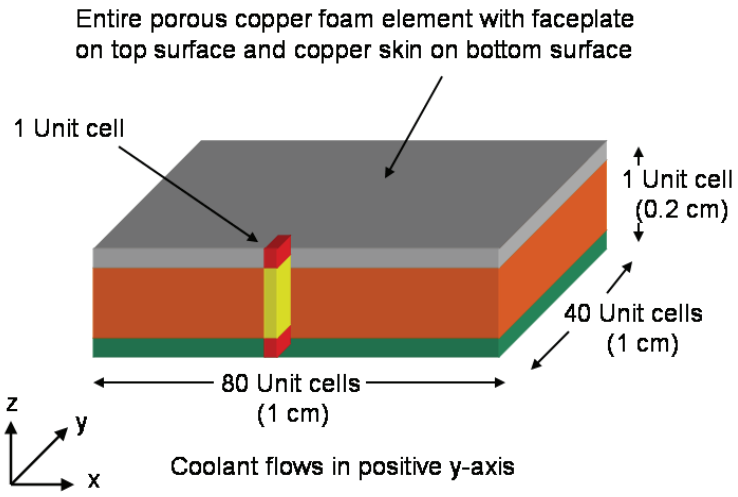

Figure 7: Unit Cell Visualization

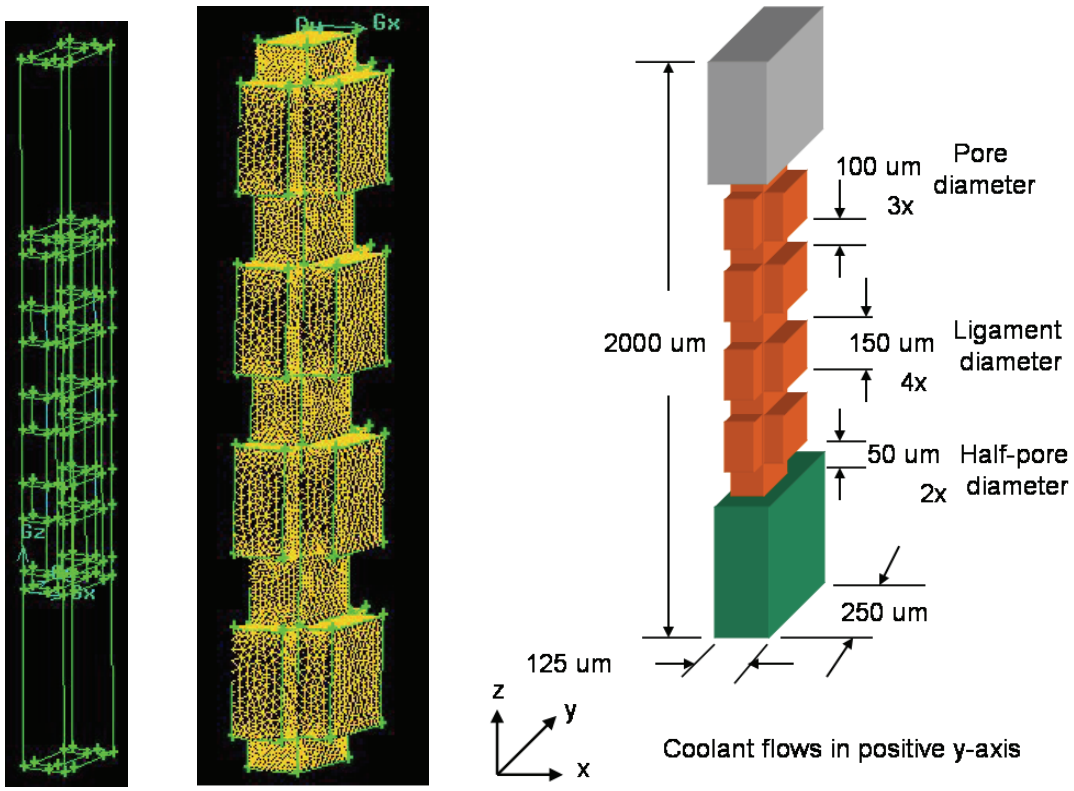

Figure 8: Ligament Diameter-Matching Unit Cell Geometry
a) Entire Model b) Mesh of Porous Copper Foam c) Unit Cell Dimensions

The model unit cell geometry, shown in Figure 9 with the applied boundary conditions, consists of four regions: the faceplate, copper ligaments, liquid water, and copper skin on the bottom surface. Three faceplate material configurations were modeled using the ligament diameter-matching model: copper silicon carbide metal matrix composite (CuSiC MMC), aluminum silicon carbide metal matrix composite (AlSiC MMC) and copper. The MMC faceplates offer a small coefficient of thermal expansion (CTE) mismatch between the faceplate and electronic components that would be mounted to it as well as the potential for improved thermal conductivity as new materials are developed. This separate study within the investigation of porous foam coldplates allows for tradeoff analysis between the faceplate-to-electronics CTE mismatch reduction offered by the MMCs and the higher thermal conductivity offered by copper. A deeper discussion of this sub-study is located in chapter 4.

In addition to the unit cell assumptions, the ligament diameter-matching model deviates from the true foam microstructure by utilizing square cross-section ligaments because of the complexity of creating model geometry with circular cross-sections and due to the computational expense of reaching convergence on such geometries. The random orientation of the ligament microstructure of the porous copper foam element is often accounted for by applying an effective thermal conductivity that is a fraction that of pure copper to the unit cell ligaments. For example, Ashby et al. employ a scaling factor λ of 0.28 [27]. The thermophysical properties of the materials used in the model are listed in Table 4, and the boundary conditions of the model are depicted in Figure 9.

Table 4: Thermophysical Properties of Materials Used in Predictive Model

Material	Density	Specific Heat	Thermal Conductivity	Viscosity
	[kg/m3]	[J/(kg-K)]	[W/(m-K)]	[kg/(m-s)]
Copper	8978	381	387.6	-
Copper Foam Ligament	8978	381	387.6 λ	-
Liquid Water	998.2	4182	0.6	0.001003
CuSiC MMC	4290	651	105	-
AlSiC MMC	3080	866.5	194.4	-

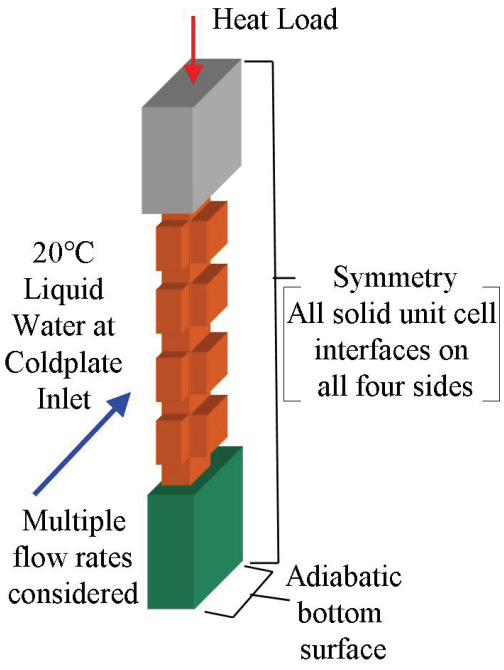

Figure 9: Model Boundary Conditions

Porosity-Matching Ligament Model

In their study of periodic unit cell models of porous foam, Boomsma et al. maintain common between the physical sample and the computational model the porosity [22]. Lu et al. developed their ligament diameter from the relative density of the foam [20]. Due to their promising results, a model which matches the porosity of the candidate foam is included in the investigation. Taking the orthogonal lattice of ligaments in the

ligament diameter-matching model, the porosity was calculated to be 35.2%. Since the candidate copper foam has a porosity of 20%, the ligaments were enlarged from 150 to 221.25 microns, and the pores were shrunk from 100 to 23 microns such that the porosity-matching geometry can be described by Figure 10. The porosity of this structure is 20.05%. This is the only difference between the ligament diameter-matching model and the porosity-matching model. The boundary conditions illustrated in Figure 9 apply.

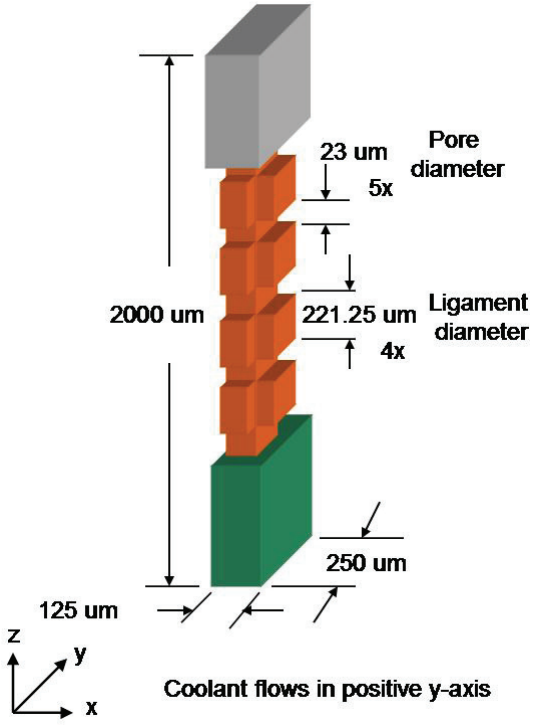

Figure 10: Porosity-Matching Unit Cell Geometry

SEM Photo-Based Model

The third and final model investigated is meant to explore a new direction compared to the previous two models. This model does not simplify the foam microstructure into an orthogonal lattice as Lu et al. suggests but instead is comprised of a wall with a thermal conductivity scaling factor λ of 1 and multiple tortuous pores of varying size and shape. This model does not have streamwise ligaments to stir the flow but does attempt to

cause mixing of the coolant due to the design of the pores. As Figure 11 shows, the model has a porosity of approximately 65%. The dark regions are the liquid zones. The design was based off of the scanning electron microscope (SEM) images found in Figures 12 and 13 which provide approximate pore and ligament dimensions and illustrate the coolant path which seems much more tortuous than that which would occur in an orthogonal lattice. The boundary conditions depicted in Figure 9 are valid for this model.

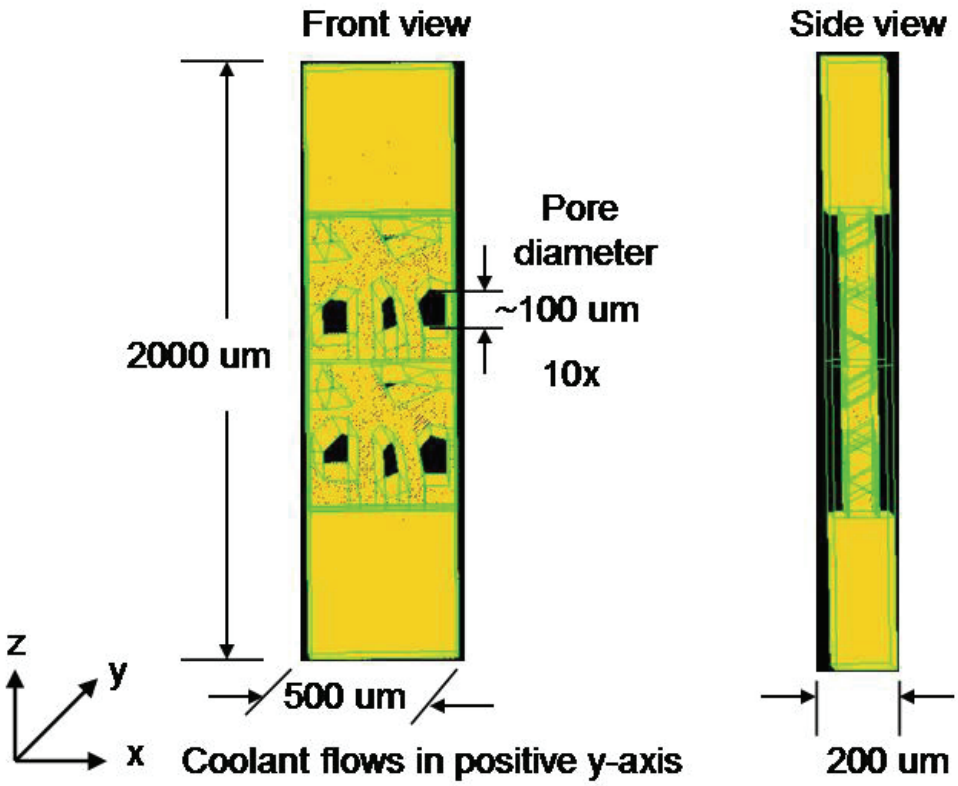

Figure 11: SEM Photo-Based Unit Cell Geometry

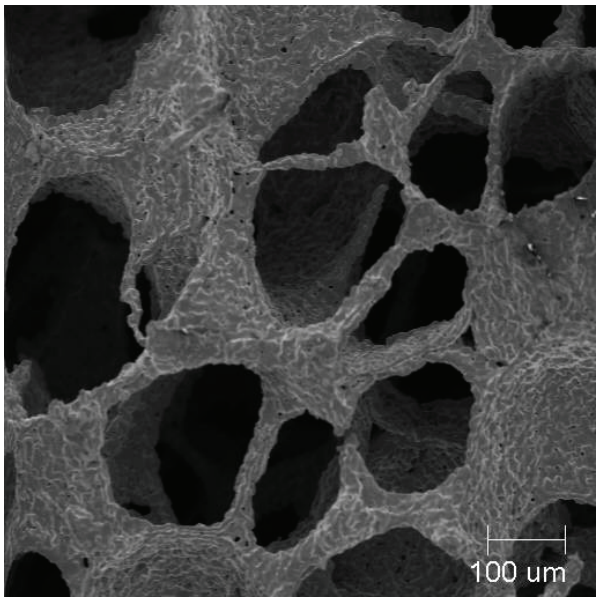

Figure 12: SEM Image 1

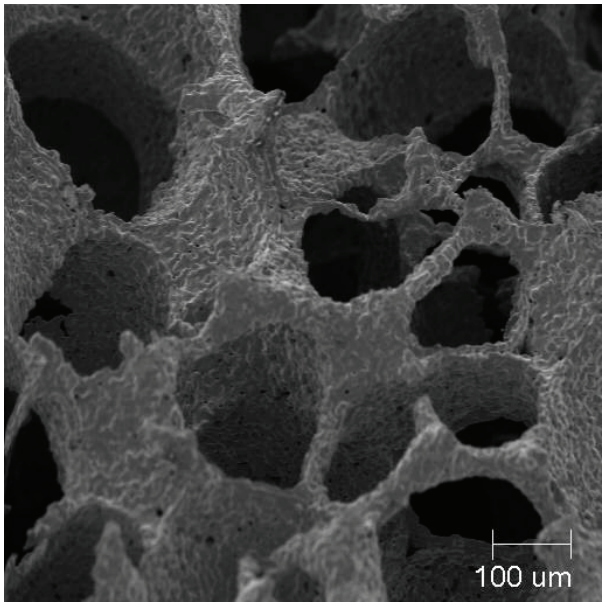

Figure 13: SEM Image 2

3.2 Experimental Characterization

A coldplate test stand was designed and constructed which supplies coolant and thermal energy to the coldplate while measuring critical temperatures and the pressure drop across the coldplate. The major issues involving the experimental evaluation include

test stand layout, component selection, attachment of a heat source to the coldplate under test, safety from electrical shock, insulation of heat sources to minimize losses to the environment, and coolant purity. The overall coldplate test stand layout, shown in Figure 14, can be divided into two regions: the coolant loop and the power electronics.

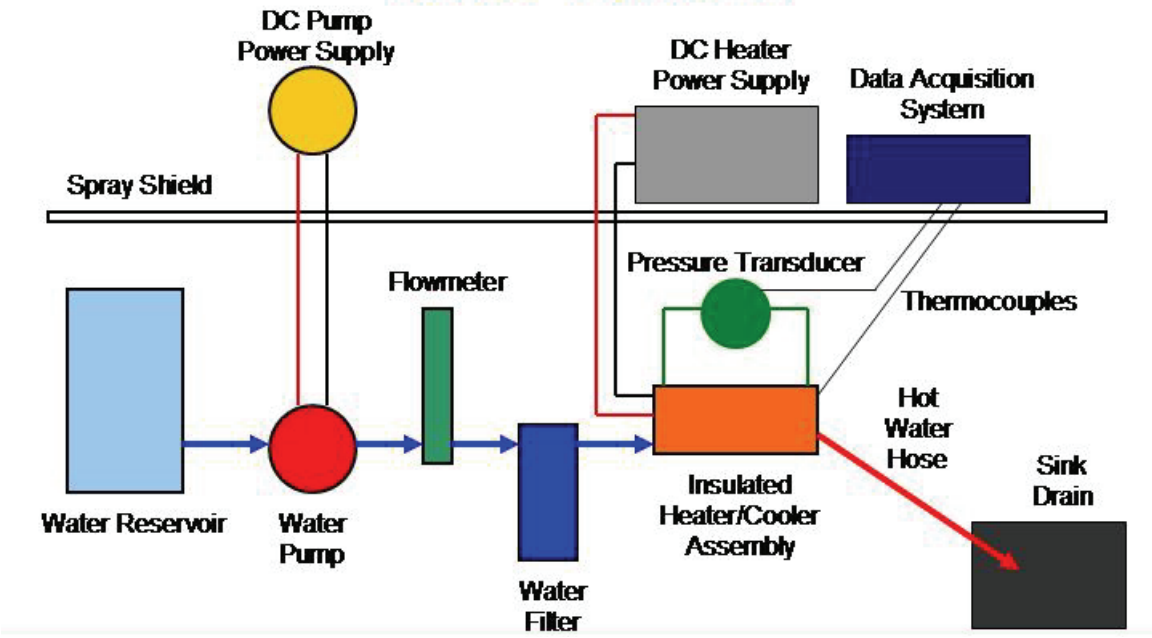

Figure 14: Coldplate Test Stand Layout

The coolant for the test loop is deionized water held in a 7.5 gallon Nalgene reservoir. The reservoir can be replenished without test interruption to allow for lengthy test durations in order to reach steady state conditions. An IDEX Micropump pump head and a DC drive motor are employed to propel the coolant through the coolant loop and overcome the pressure restriction of the coldplate. A DC power supply allows for flow rate adjustment. Key features of the gear pump head include its magnetic drive, suction shoe design, and 125 psi maximum pressure differential. After exiting the pump, the coolant flow travels through ¼-inch-diameter copper tubing to a variable area flowmeter which has a range of 3.2×10^{-7} to 8.4×10^{-6} m^3/s [19 to 506 mL/min]. The coolant

proceeds through the 1-micron water filter. The deionized water is filtered directly before its entrance into the coldplate in order to remove impurities possibly added by the tank, pump, or flowmeter. Once filtered, the coolant flow is split into two paths at a cross in the tubing to provide a more uniform flow through the coldplate. Once the coolant passes through the coldplate, it exits via two outlet tubes identical to the inlet plumbing which join in a cross. The cross is attached to a Teflon-lined braided stainless steel drain hose which empties into a sink drain. The drain hose was chosen for its high temperature rating to allow for the possibility of boiling coolant exiting the coldplate.

No heat sources with 1 cm^2 of surface area were found which could produce 1 kilowatt of thermal energy. Therefore, a copper heat-focusing block was machined which concentrates the thermal energy injected into the larger top face through the block and out the smaller bottom face which has 1 cm^2 of surface area. In order to minimize the required maximum heater temperature, solder with a melting temperature of 305°C was used to attach the coldplate to the smaller bottom face of the heat-focusing block as well as to attach the eight heaters to the larger top face of said block. Eight strip heaters that produce 125 W each were chosen due to their maximum temperature rating of 815°C and their Incoloy nickel alloy surface finish. Such a finish is believed to have a higher probability of good solder wetting than the standard stainless steel strip heaters on the market. In order to minimize the strain on the solder joint between the heat-focusing block and the coldplate caused by the moment of the top-heavy heat-focusing block, adjustable balancing screws with sharpened contact points bear the load of the heat-focusing block. The screws thread into a steel plate chosen for its low thermal conductivity. A key design feature of the heater/coldplate assembly is the cocoon of high temperature calcium silicate insulation around the surfaces of the heat-focusing block and the heaters to minimize the amount of heat that is not channeled into the

coldplate. Fiberglass paper was used to fill the gaps between the calcium silicate pieces. It was also employed to insulate the copper tubing which connects the coldplate to the drain hose and to insulate the thermocouple which measures the coolant temperature exiting the coldplate. The heater input power is generated by an Agilent 120 V/18 A DC power supply and routed through two distribution bus bars to the eight strip heaters. For safety reasons, the coolant loop was isolated as much as possible from the test stand power electronics. A plexiglass spray shield sits between the coolant loop and the electronics to prevent a potential pressurized leak from spraying water on the high-power electronics. A system leak is not expected and did not occur during testing, but the necessary safety precautions have been taken.

In order to minimize the heater temperature for a given heat flux, the thermal resistance of the heat-focusing block was optimized via 9 design iterations each evaluated with a Fluent predictive model. The final design incorporates 3 cross-sectional reductions as it shrinks from the large top surface area used for heater attachment to the 1 cm^2 lower surface area used for coldplate attachment, as shown in Figure 15. Figure 16 depicts the analysis results of the final design in Kelvin units. A total heat flux of 1 kW/cm^2 from the eight strip heaters was applied in their footprints on the top surface of the block. The temperature of the face of the block which would contact the coldplate was fixed at 125°C, and the maximum area-averaged temperature where the heater is attached was monitored. The final design was chosen because it was the smallest volume heat-focusing block which would not exceed the 305°C heater area maximum temperature dictated by the solder melting temperature. The model reported a maximum heater area temperature of 298.9°C.

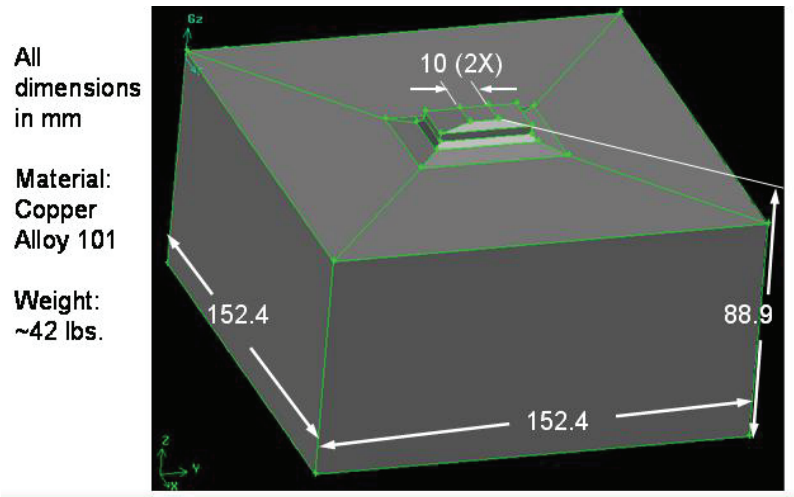

Figure 15: Optimized Design of Heat-Focusing Block

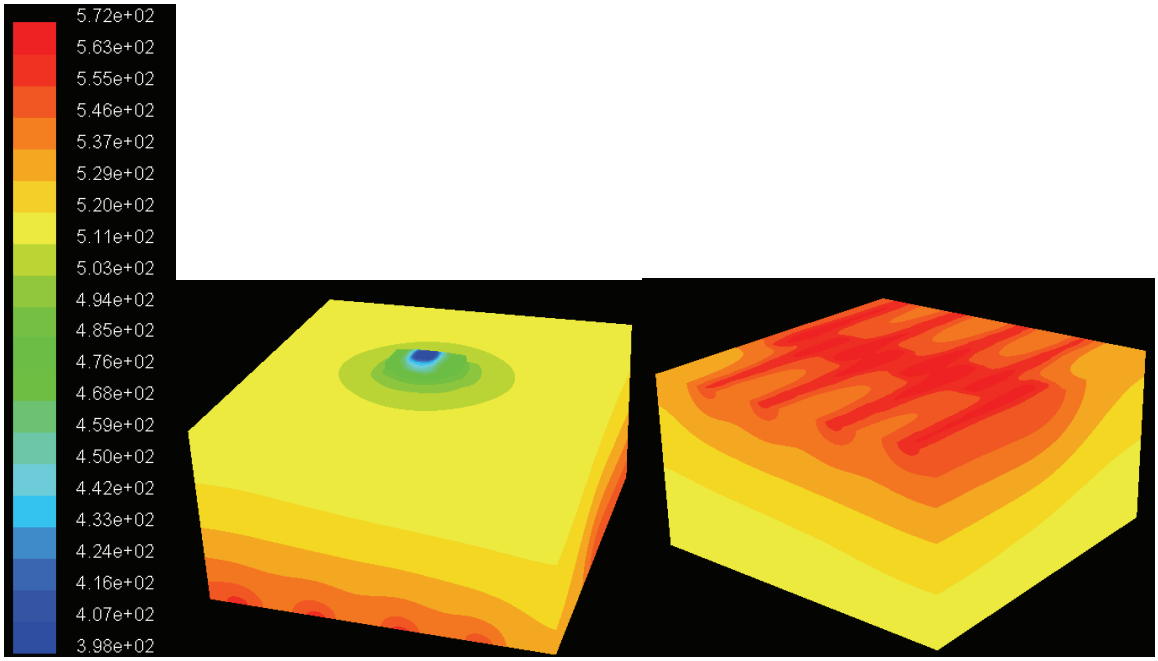

a) b)

Figure 16: Heat-Focusing Block Thermal Results
a) Coldplate Mounting Side b) Heater Mounting Side

Five thermocouple measurements and one differential pressure measurement are taken every 5 seconds during an experimental evaluation. The thermocouples are mounted in the following locations:

- Coldplate faceplate near downstream edge of heat application
- Coolant inlet to coldplate
- Coolant exit from coldplate
- Ambient air surrounding coldplate inside insulation cocoon
- Heater casing temperature

The pressure drop across the coldplate is measured via pressure taps integrated into the coldplate housing using a differential pressure transducer and captured by the data acquisition system. The data acquisition system consists of an Agilent data acquisition switch unit, a desktop PC, and an Agilent PC interface card.

CHAPTER 4

RESULTS

4.1 Computational Modeling

The three periodic unit cell geometry construction techniques will first be compared with experimental results from a coldplate characterization in which coolant bypass occurred. After presenting the overall comparison of model performance, the impact of coldplate faceplate thermal conductivity will be discussed, and the coolant bypass which occurred during the experimental evaluation will be investigated further.

The thermal resistance of the foam coldplate will be the parameter used to measure the accuracy of the computational model. Due to difficulty with coolant bypass at the foam element, experimental pressure drop measurements are not available to compare with the model predictions for pressure drop. The thermal resistance will be defined by equation (4):

$$R_{Thermal} = \frac{T_{Max} - T_{Coldplate\ Inlet}}{\dot{m} c_p \left(T_{Coldplate\ Exit} - T_{Coldplate\ Inlet} \right)} \tag{4}$$

The maximum faceplate temperature is calculated using equation (5) :

$$T_{Max} = T_{Unit\ cell\ foam\ top} + \left[T_{Unit\ cell\ exit} - T_{Coldplate\ Inlet} \right] * \left[N_{Unit\ cell} - 1 \right] + \left[\frac{q'' L_{Faceplate\ thickness}}{k_{Faceplate}} \right] \tag{5}$$

The coldplate exit temperature is calculated using equation (6):

$$T_{Coldplate\ Exit} = T_{Unit\ cell\ exit} + \left[T_{Unit\ cell\ exit} - T_{Coldplate\ Inlet} \right] * \left[N_{Unit\ cell} - 1 \right] \tag{6}$$

On the coldplate, the maximum faceplate temperature is predicted to occur at the trailing edge of the heated region due to the continual addition of thermal energy to the coolant from the faceplate and copper foam as the coolant flows through the coldplate as shown in Figure 17.

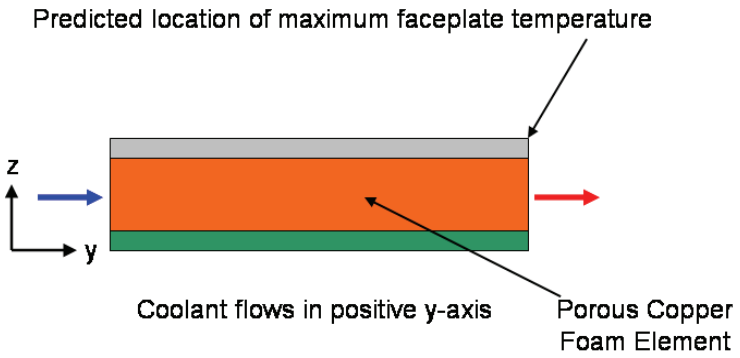

Figure 17: Maximum Faceplate Temperature Location

Figures 18, 19, and 20 depict the thermal resistance prediction by the ligament diameter-matching model, porosity-matching model, and SEM photo-based model respectively. The data depicted in Figures 18, 19, and 20 is tabulated in Table 5. Collectively the models predicted thermal resistances in the range of 0.07 to 0.23 °C/W for the flow and heat flux scenarios considered. The experimental characterization yielded similar thermal resistance measurements in the range of 0.09 to 0.25 °C/W despite experiencing coolant bypass.

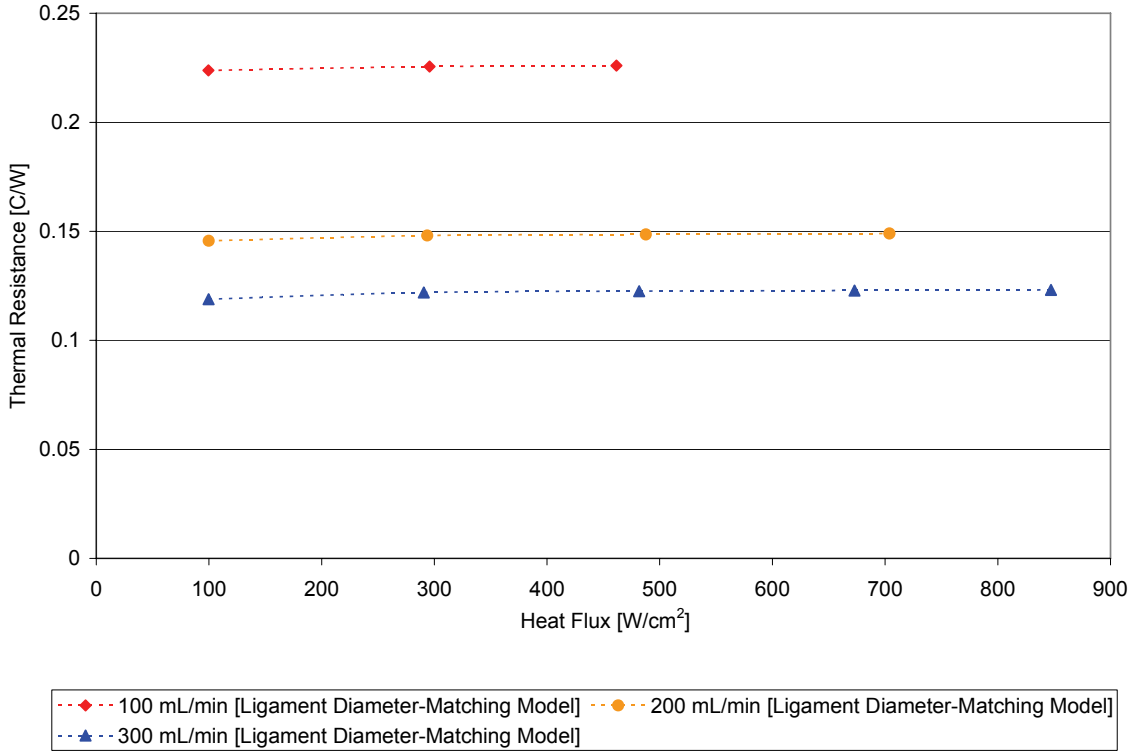

Figure 18: Thermal Resistance Prediction by Ligament Diameter-Matching Model

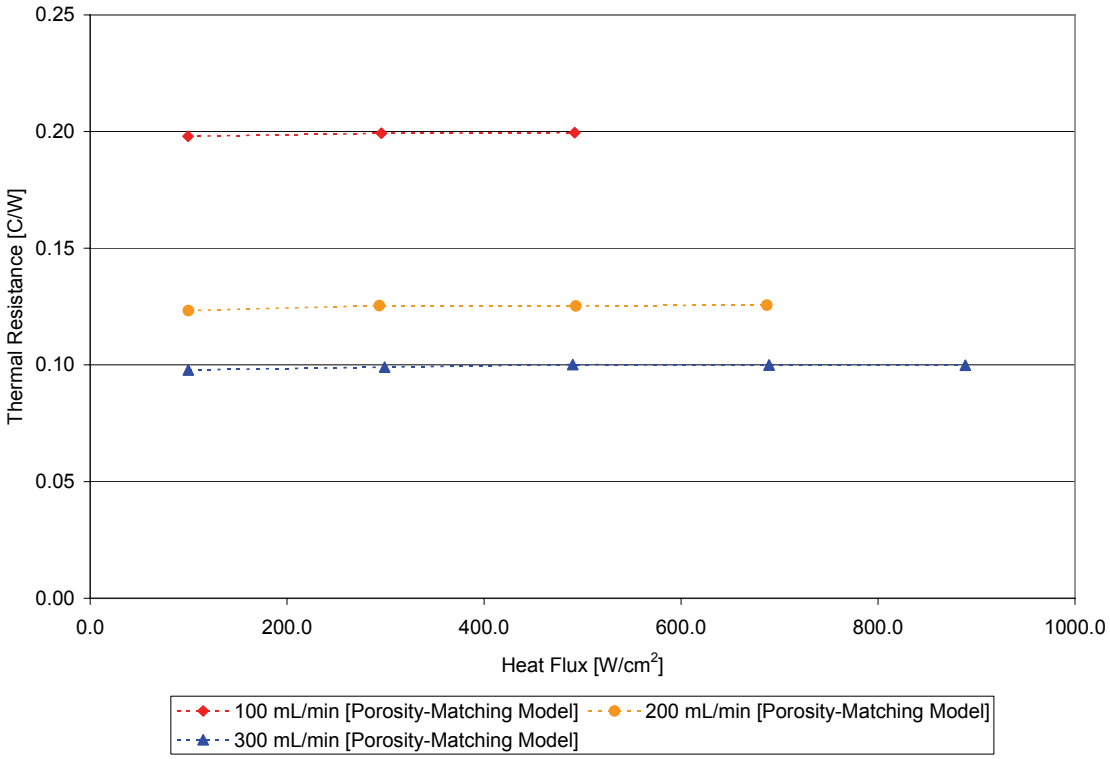

Figure 19: Thermal Resistance Prediction by Porosity-Matching Model

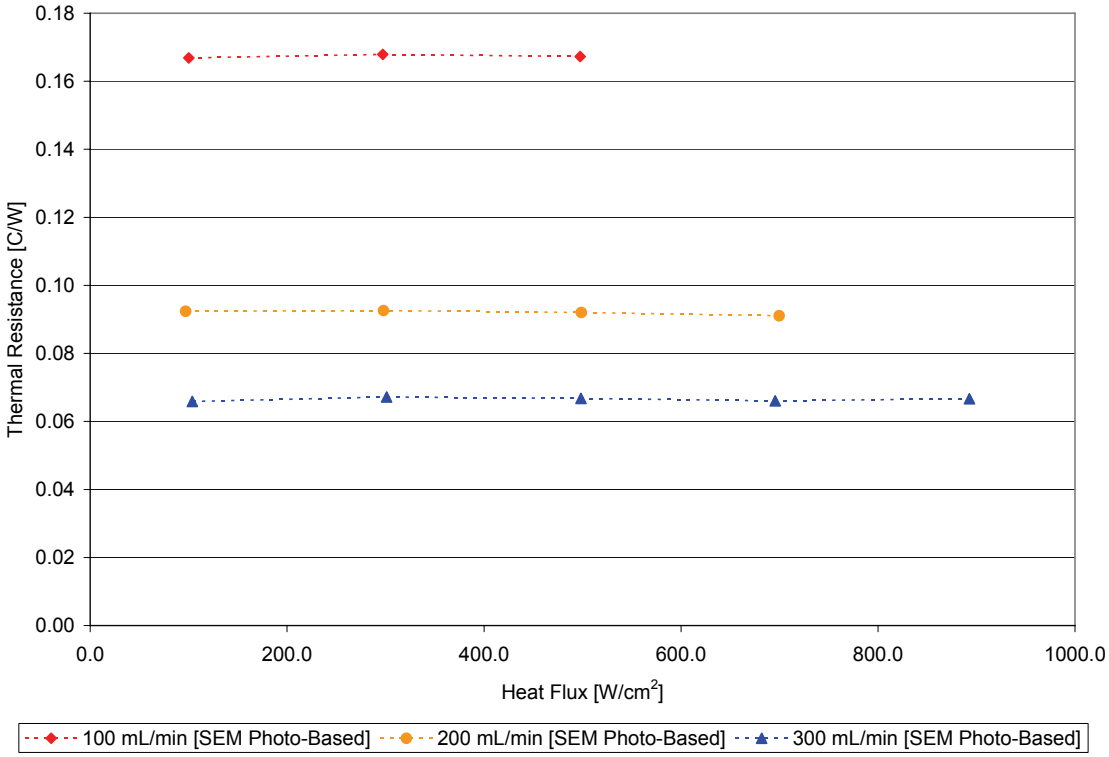

Figure 20: Thermal Resistance Prediction by SEM Photo-Based Model

Table 5: Thermal Resistance Results from Models and Experimental Data

Heat Input to Water	Cooler Faceplate Temp	Heater Temp	Input Electrical Power	Water Flow Rate	Inlet Water Temp	Exit Water Temp	Thermal Resistance
[W]	[C]	[C]	[W]	[mL/min]	[C]	[C]	[C/W]
Experimental							
105.1	48.2	153.5	161.6	101.0	21.5	36.6	0.25
200.7	55.1	269.4	321.1	101.0	21.3	50.0	0.17
233.1	63.9	297.2	373.3	101.0	20.4	53.7	0.19
104.0	34.4	143.7	155.2	198.4	22.1	29.7	0.12
202.8	47.0	246.1	288.4	198.4	22.8	37.6	0.12
262.6	48.6	296.1	387.4	198.4	21.9	41.0	0.10
100.1	30.3	126.0	124.9	299.3	19.3	24.2	0.11
193.5	40.1	222.2	280.6	299.3	18.6	27.9	0.11
290.9	46.1	298.2	395.6	299.3	20.2	34.3	0.09
Modeling							
Ligament-Based							
99.5	42.3	-	-	99.8	20.0	34.4	0.22
295.8	86.7	-	-	99.8	20.0	62.8	0.23
461.6	124.3	-	-	99.8	20.0	86.8	0.23
99.8	34.5	-	-	200.2	20.0	27.2	0.15
293.7	63.5	-	-	200.2	20.0	41.2	0.15
487.7	92.4	-	-	200.2	20.0	55.2	0.15
703.8	124.9	-	-	200.2	20.0	70.8	0.15
99.7	31.8	-	-	300.0	20.0	24.8	0.12
290.7	55.4	-	-	300.0	20.0	34	0.12
481.7	79.0	-	-	300.0	20.0	43.2	0.12
672.8	102.6	-	-	300.0	20.0	52.4	0.12
847.2	124.4	-	-	300.0	20.0	60.8	0.12

Table 5 (continued)

Heat Input to Water	Cooler Faceplate Temp	Heater Temp	Input Electrical Power	Water Flow Rate	Inlet Water Temp	Exit Water Temp	Thermal Resistance
[W]	[C]	[C]	[W]	[mL/min]	[C]	[C]	[C/W]
Modeling							
Porosity-Based							
99.5	39.7	-	-	99.8	20.0	34.4	0.20
295.8	78.9	-	-	99.8	20.0	62.8	0.20
492.0	118.2			99.8	20.0	91.2	0.20
99.8	32.3	-	-	200.2	20.0	27.2	0.12
293.7	56.8	-	-	200.2	20.0	41.2	0.13
493.2	81.8	-	-	200.2	20.0	55.6	0.13
687.2	106.3			200.2	20.0	69.6	0.13
99.7	29.7	-	-	300.0	20.0	24.8	0.10
299.0	49.6	-	-	300.0	20.0	34.4	0.10
490.0	69.1	-	-	300.0	20.0	43.6	0.10
689.4	88.9	-	-	300.0	20.0	53.2	0.10
888.7	108.8	-	-	300.0	20.0	62.8	0.10
SEM Photo-Based							
100.2	36.7	-	-	99.8	20.0	34.5	0.17
297.2	69.9	-	-	99.8	20.0	63.0	0.17
497.6	103.2	-	-	99.8	20.0	92.0	0.17
97.0	29.0	-	-	200.2	20.0	27.0	0.09
297.9	47.6	-	-	200.2	20.0	41.5	0.09
498.8	65.9	-	-	200.2	20.0	56.0	0.09
699.6	83.7	-	-	200.2	20.0	70.5	0.09
103.8	26.8	-	-	300.0	20.0	25.0	0.07
301.1	40.2	-	-	300.0	20.0	34.5	0.07
498.4	53.3	-	-	300.0	20.0	44.0	0.07
695.6	65.9	-	-	300.0	20.0	53.5	0.07
892.9	79.5	-	-	300.0	20.0	63.0	0.07

A study of effective thermal conductivity of the foam microstructure geometry was undertaken to determine how the scaling factor for the 100 ppi copper foam compares to Evans' 0.28 scaling factor for ERG foam. Because the models do not account for the coolant bypass which occurred in the experimental characterization, the modeling results provide a lower bound for coldplate thermal resistance or best case scenario. This lower bound would be realized when the effect of the coolant bypass on the coldplate performance was minimal. Focusing on the case of a coolant flow rate of 200 mL/min and an applied heat flux of 100 W/cm^2, Figure 21 compares the thermal resistance measured experimentally to that of the ligament diameter-matching and porosity matching models employing various foam thermal conductivity scaling factors as well as the SEM photo-based model.

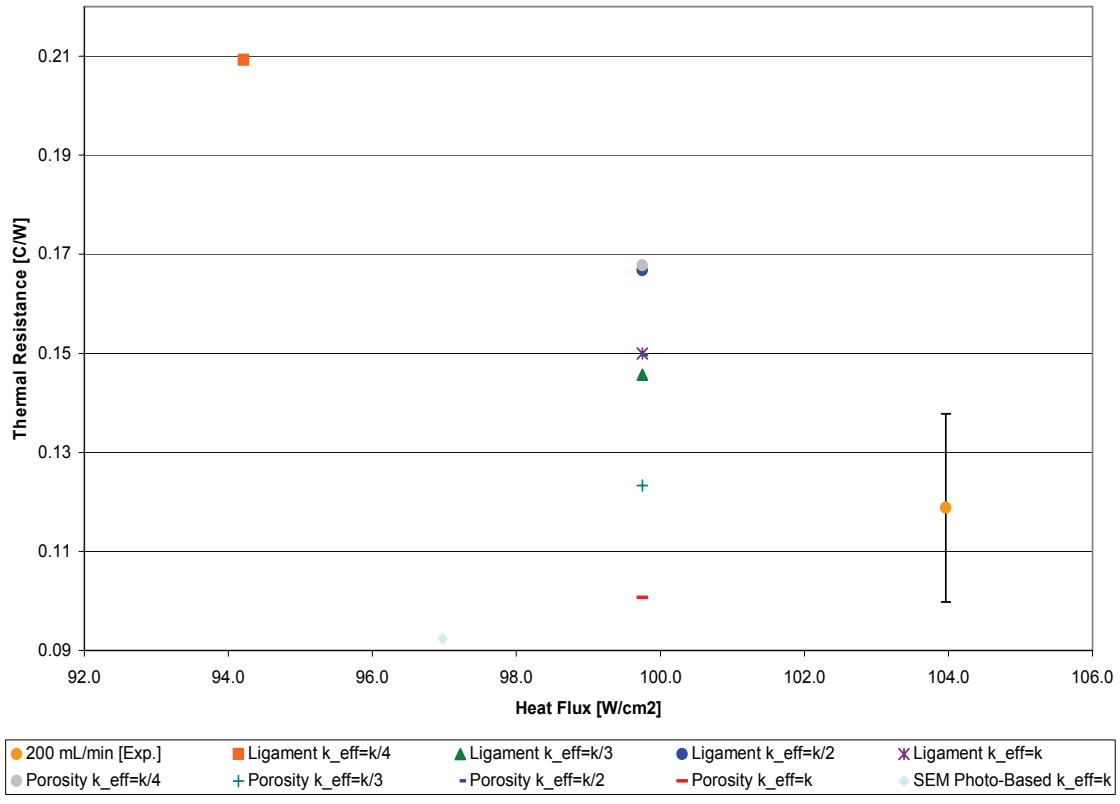

Figure 21: Foam Effective Thermal Conductivity Evaluation
Via Thermal Resistance Prediction

From Figure 21, one can see that a porosity-matching ligament model using a scaling factor of 0.33 is the combination of modeling technique and scaling factor evaluated in this study for the 100 ppi candidate foam which most closely matches the experimental performance during coolant bypass. A porosity-matching ligament model with a scaling factor of 1 is the modeling approach with the second best match of the experimental data; whereas the thermal resistance prediction of the ligament diameter-matching model and the SEM photo-based model did not fall within the bounds of the experimental data. The data depicted in Figure 21 is tabulated in Table 6. While the above-mentioned modeling approaches match well the experimental results, these results can not be accurately applied to scenarios with different coolant bypass phenomenon. To accurately predict the effective thermal conductivity of the foam element experiencing coolant bypass, said bypass would need to be incorporated into the computational model. To determine the physics behind why the porosity-matched model achieves a low thermal resistance similar to the experimental data, the velocity and temperature fields constructed in Fluent will now be analyzed.

Table 6: Foam Effective Thermal Conductivity Evaluation
Via Thermal Resistance Prediction

Heat Input to Water	Cooler Faceplate Temp	Heater Temp	Input Electrical Power	Water Flow Rate	Inlet Water Temp	Exit Water Temp	Thermal Resistance
[W]	[C]	[C]	[W]	[mL/min]	[C]	[C]	[C/W]
Experimental							
105.1	48.2	153.5	161.6	101.0	21.5	36.6	0.25
200.7	55.1	269.4	321.1	101.0	21.3	50.0	0.17
233.1	63.9	297.2	373.3	101.0	20.4	53.7	0.19
104.0	34.4	143.7	155.2	198.4	22.1	29.7	0.12
202.8	47.0	246.1	288.4	198.4	22.8	37.6	0.12
262.6	48.6	296.1	387.4	198.4	21.9	41.0	0.10
100.1	30.3	126.0	124.9	299.3	19.3	24.2	0.11
193.5	40.1	222.2	280.6	299.3	18.6	27.9	0.11
290.9	46.1	298.2	395.6	299.3	20.2	34.3	0.09
Modeling							
Effective Thermal Conductivity							
Ligament k_eff=k/4							
94.2	39.7	-	-	200.2	20.0	26.8	0.21
Ligament k_eff=k/3							
99.8	34.5	-	-	200.2	20.0	27.2	0.15
Ligament k_eff=k/2							
99.8	36.6	-	-	200.2	20.0	27.2	0.17
Ligament k_eff=k							
99.8	35.0	-	-	200.2	20.0	27.2	0.15
Porosity k_eff=k/4							
99.8	36.7	-	-	200.2	20.0	27.2	0.17
Porosity k_eff=k/3							
99.8	32.3	-	-	200.2	20.0	27.2	0.12
Porosity k_eff=k/2							
99.8	34.9	-	-	200.2	20.0	27.2	0.15
Porosity k_eff=k							
99.8	30.0	-	-	200.2	20.0	27.2	0.10
SEM Photo-Based k_eff=k							
97.0	29.0	-	-	200.2	20.0	27.0	0.09

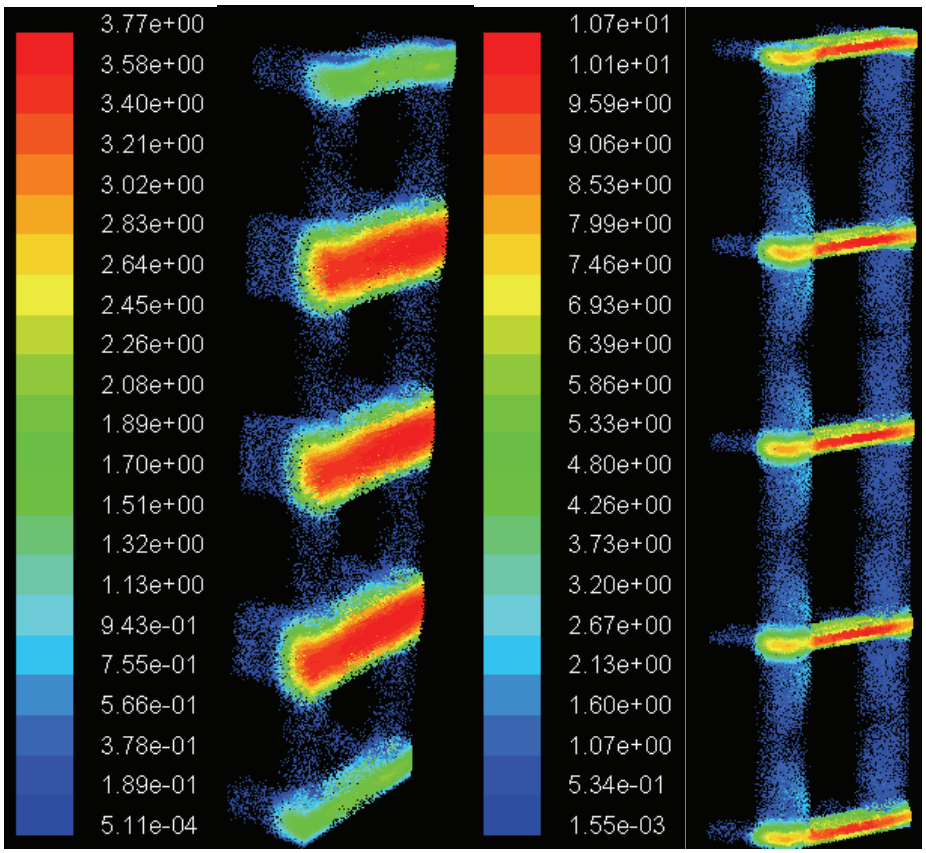

a) b)

Figure 22: Velocity Vector Fields (200 mL/min)
a) Ligament Diameter-Matching Model b) Porosity-Matching Model

In Figure 22, the velocity vector fields of the ligament diameter-matching model and the porosity-matching model for the 200 mL/min case are depicted. Studying the vector fields we are reminded that the hydraulic diameter of the pores in the porosity-matching model is 37.4 microns; whereas, the pores of the ligament diameter-matching model have a hydraulic diameter of 100 microns, according to equation (7) [28].

$$D_h = \frac{4A_{cross}}{P} \tag{7}$$

Applying equations (8) and (9) below, the hydrodynamic and thermal entrance lengths are found for both models to occur in less than 5 mm except for the 300 mL/min flow rate

through the ligament diameter-matching model which requires 12 mm [28]. This also justifies the fully-developed flow assumption required by the periodic unit cell construction.

$$x_{fd,h} = 0.05\,\mathrm{Re}_D\,D_h \tag{8}$$

$$x_{fd,t} = 0.05\,\mathrm{Re}_D\,\mathrm{Pr}\,D_h \tag{9}$$

In addition, this information also confirms that the fully-developed laminar case is almost always reasonable for the 10 mm porous foam element. Considering the pore as a circular tube experiencing fully-developed laminar internal flow, the convective heat transfer coefficient behaves according to equation (10), which when evaluated for the hydraulic diameters mentioned above yields equations in the form of equation (11) for the ligament diameter-matching model and equation (12) for the porosity-matching model.

$$h = \frac{48}{11}\frac{k_{Coolant}}{D_h} \tag{10}$$

$$h = 43636k_{Coolant} \tag{11}$$

$$h = 116675k_{Coolant} \tag{12}$$

This difference in convective heat transfer coefficient through the pores of the orthogonal lattice of ligaments is a plausible answer to why the porosity-matching model has a lower thermal resistance compared to the other models. Figure 23 shows the thermal field of the SEM unit cell inlet face after convergence and the velocity vector field as seen from the side of the model where the pore structure can best be visualized. The range of velocities seen in the pores testifies to the tortuous path the pores force.

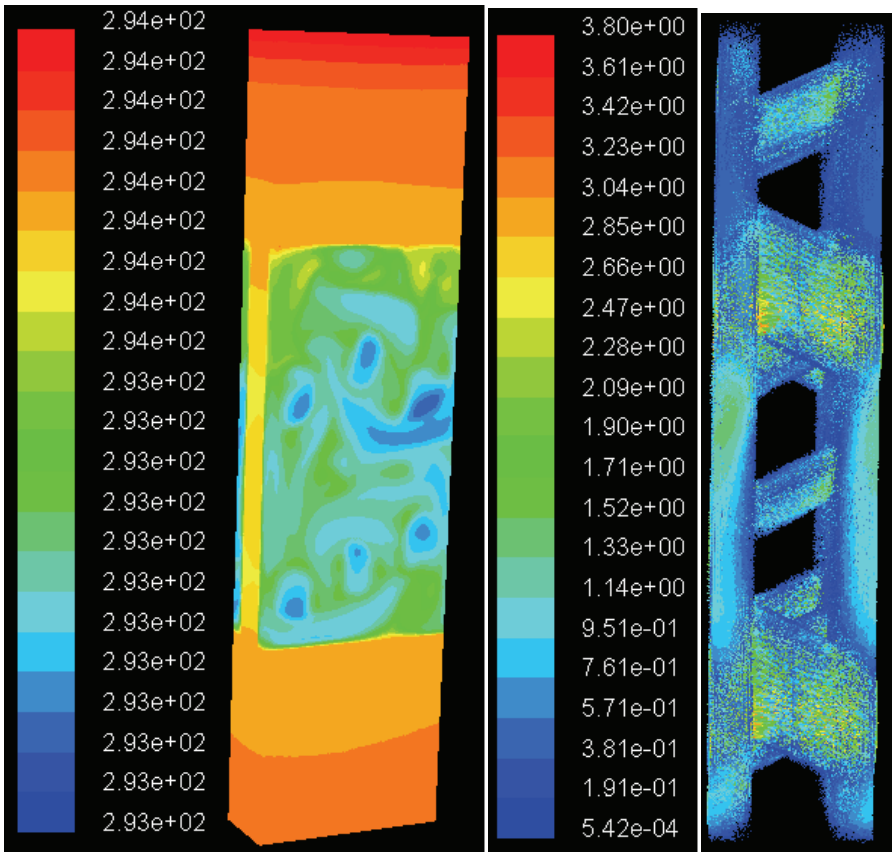

a) b)

Figure 23: Thermofluid Fields for SEM Photo-Based Model (200 mL/min 100 W/cm^2)
a) Temperature Field at Unit Cell Exit b) Velocity Vector Field (Side View)

In Figure 24, images are provided which depict the temperature fields of the model which best predicted the experimental value of the thermal resistance of the coldplate for the case of 200 mL/min and 100 W/cm^2, the porosity-matching model with a λ of 0.33.

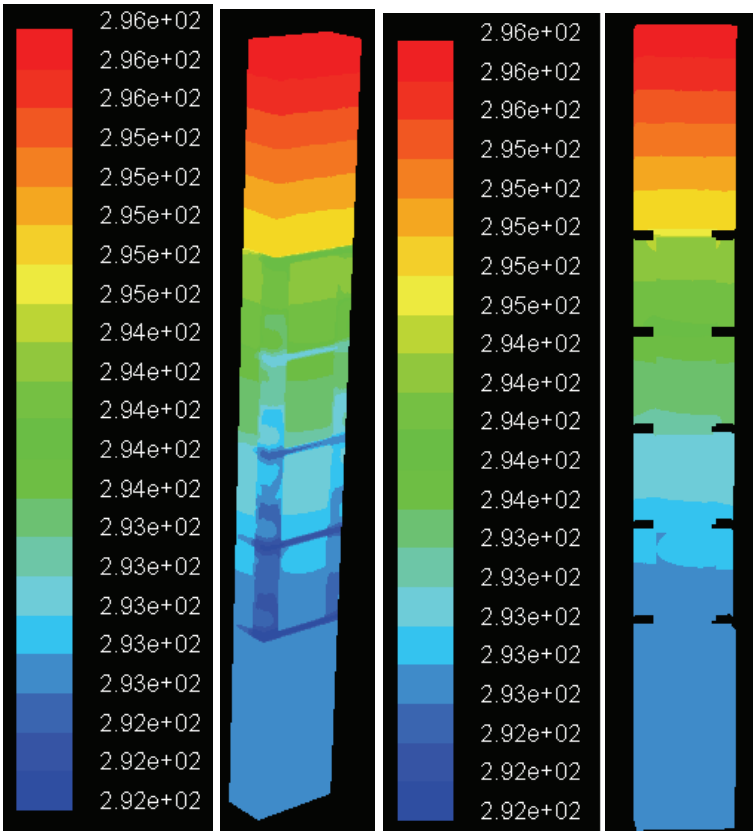

a) b)

Figure 24: Temperature Fields of Porosity-Matching Model
λ=0.33 (200 mL/min 100 W/cm^2)
a) Foam and Coolant b) Foam Only

The relationship between the coldplate pressure drop and coolant flow rate is shown in Figure 25 as predicted by the unit cell models for the range of approximately 1.7x10^{-6} to 5x10^{-6} m^3/s [100 to 300 mL/min] for the boundary conditions detailed in Figure 9. Interestingly, the ligament diameter-matching model and the SEM photo-based model predictions are much closer to each other than that of the porosity-matching model. Unfortunately, due to coolant bypass, no accurate experimental pressure drop data is available to compare with the computational predictions.

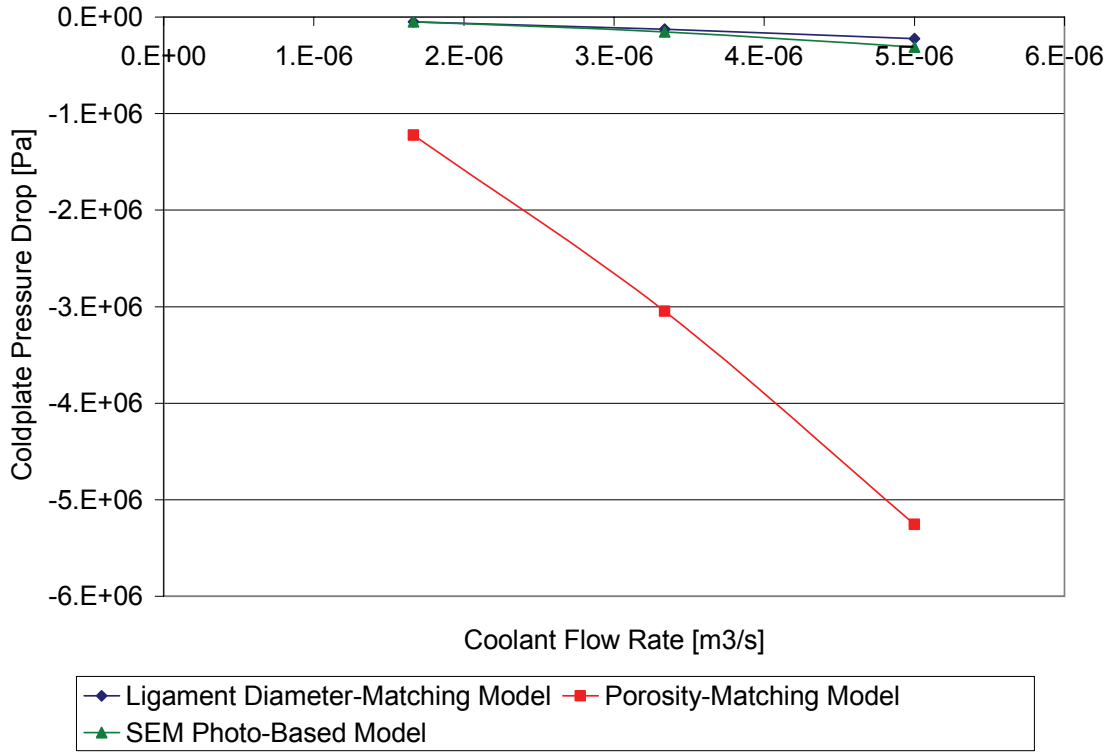

Figure 25: Coldplate Pressure Drop vs. Coolant Flow Rate

A pressure correction equation is derived from the continuity equation to couple the pressure and velocity of the flow and force conservation of mass. The residual of the pressure correction equation is a parameter which can be used to gauge the convergence of the momentum equation solution. Table 7 contains the pressure correction equation residuals recorded at the final iteration for each of the Fluent cases evaluated.

Table 7: Pressure Correction Equation Residuals

Modeling Approach	Flow rate	Heat flux	λ	Pressure Correction Equation Residual
	[mL/min]	[W/cm^2]	-	-
A	100	100	0.33	8.51E-12
		300	0.33	4.96E-12
		500	0.33	2.06E-09
	200	100	0.33	1.41E-10
		300	0.33	1.96E-10
		500	0.33	1.96E-10
		700	0.33	1.24E-09
	300	100	0.33	1.56E-11
		300	0.33	1.59E-11
		500	0.33	1.59E-11
		700	0.33	1.36E-11
		900	0.33	2.38E-10
B	100	100	0.33	3.64E-11
		300	0.33	1.04E-10
		500	0.33	3.13E-09
	200	100	0.33	2.95E-07
		300	0.33	4.38E-09
		500	0.33	2.73E-09
		700	0.33	8.97E-08
	300	100	0.33	9.71E-09
		300	0.33	9.71E-09
		500	0.33	9.70E-09
		700	0.33	7.99E-08
		900	0.33	9.70E-09
C	100	100	1.00	3.12E-08
		300	1.00	3.34E-09
		500	1.00	1.66E-09
	200	100	1.00	2.73E-08
		300	1.00	2.31E-08
		500	1.00	4.91E-10
		700	1.00	2.11E-05
	300	100	1.00	1.78E-07
		300	1.00	8.23E-09
		500	1.00	5.11E-08
		700	1.00	4.43E-05
		900	1.00	3.64E-07
A	200	100	0.25	1.56E-09
		100	0.33	1.41E-10
		100	0.50	1.56E-09
		100	1.00	1.70E-09
B	200	100	0.25	1.48E-09
		100	0.33	2.95E-07
		100	0.50	1.48E-09
		100	1.00	2.24E-06
C	200	100	1.00	2.73E-08

The computational grid was evaluated for grid size sensitivity. The results of this study are listed in Table 8. The relationship between the cell count and the energy balanced did not behave as expected for the ligament diameter-matching model in that the energy loss was directly proportional to the cell count instead of an inversely proportional relationship. A potential cause of this unexpected result is the difference in meshing schemes. A meshing scheme based on the shortest edge of the model geometry was used for the generation of the fine and course meshes; whereas, an interval count was specified for each edge of the models used for the research investigation.

Table 8: Grid Size Sensitivity Study

	Ligament			Porosity		
	Fine	Original	Coarse	Fine	Original	Coarse
Cell Count	426801	211501	120323	1318757	618785	265349
Energy Balance	4.02%	2.10%	0.33%	0.33%	2.10%	2.18%
Max. Facet Temp. [K]	315.84	300.54	315.60	312.94	309.21	309.65
Max. Facet Velocity [m/s]	3.81	3.77	3.50	10.59	10.66	9.13
Change in Max. Temperature	5.09%	-	5.01%	1.21%	-	0.14%
Change in Max. Velocity	1.01%	-	-7.14%	-0.62%	-	-14.29%

Studies of Faceplate Thermal Conductivity and Coolant Bypass

The ligament diameter-matching model of the coldplate was used to predict the maximum heat flux dissipated and coolant pressure drop for multiple coolant flow rates in the range of approximately 1.7×10^{-6} to 8.3×10^{-6} m^3/s [100 to 500 mL/min]. Coolant bypass which occurred in the experimental evaluation was also studied using the ligament diameter-matching model. These studies are presented with the understanding that their greatest value lies in A-B comparison and not in absolute solution determination.

Maximum heat flux dissipated is determined iteratively by increasing the dissipated power until the maximum faceplate temperature reaches 125°C for a given coolant flow rate. This maximum faceplate temperature was chosen to align with the maximum operating temperature of many power electronics components. For the coldplate under consideration, eighty ligament diameter-matching unit cells fit across the width of the copper foam element, and forty repeat in the coolant flow direction. In relation to coolant flow rate, this means that model results are multiplied by eighty to calculate the coldplate requirement. In relation to pressure drop in the direction of coolant flow, this means that model results are multiplied by forty to calculate the coldplate performance.

FACEPLATE THERMAL CONDUCTIVITY STUDY

The relationship between maximum faceplate temperature and coolant flow rate is shown in Figure 26 for all three faceplate materials across the range of approximately 3.3×10^{-6} to 8.3×10^{-6} m^3/s [200 to 500 mL/min] for the boundary conditions detailed in Figure 9 and an applied heat flux of 1 kW/cm^2.

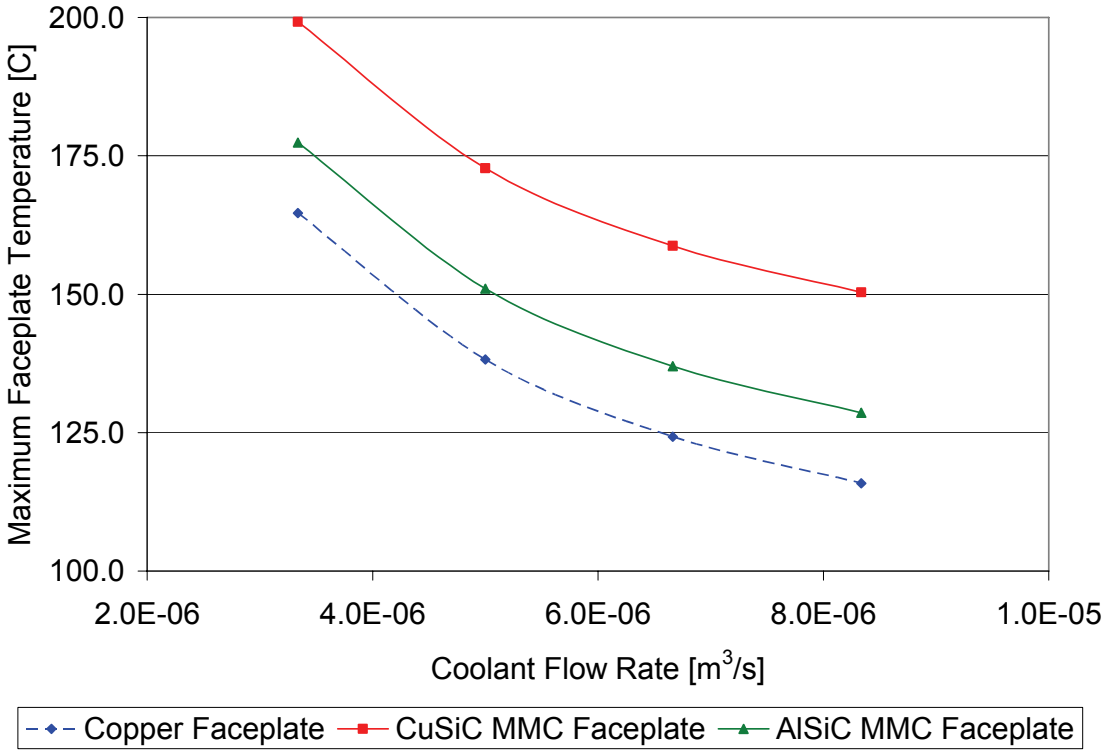

Figure 26: Faceplate Thermal Conductivity Study:
Maximum Faceplate Temperature vs. Coolant Flow Rate

The temperature field for the coldplate with the copper faceplate and a 7.0×10^{-6} m^3/s [400 mL/min] coolant flow rate is found in Figure 27 a). The temperature field for the coldplate with the CuSiC MMC faceplate and the coldplate with the AlSiC MMC faceplate at the same coolant flow rate are depicted in Figure 27 b) and 28 respectively. All three plots display temperatures in Kelvin.

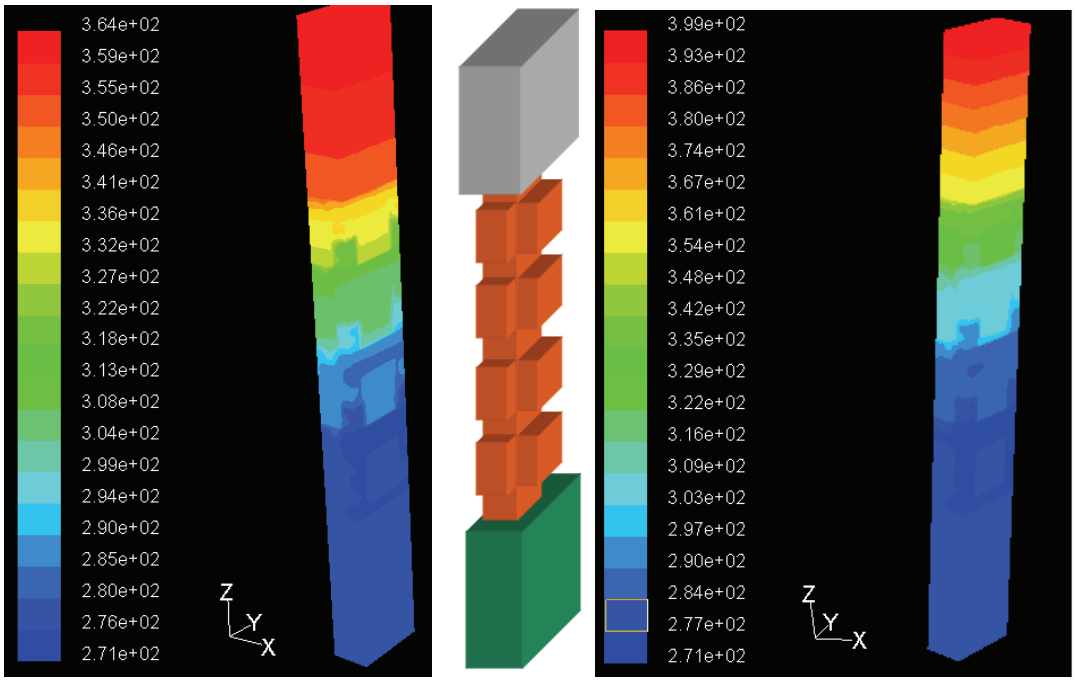

a) b)

Figure 27: Temperature Field (400 mL/min Flow Rate)
a) Coldplate with Copper Faceplate b) Coldplate with CuSiC Faceplate

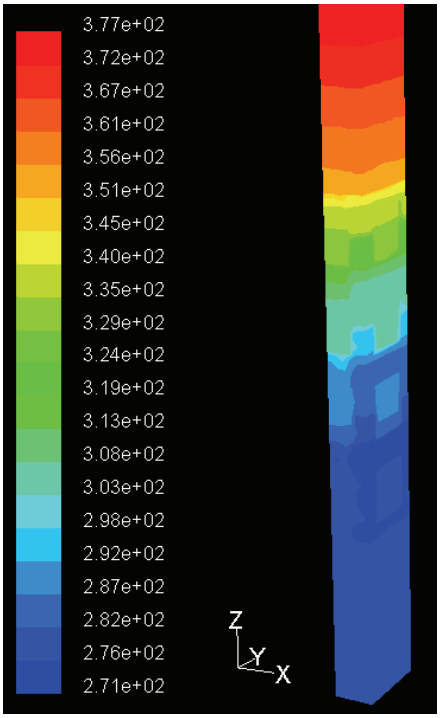

Figure 28: Temperature Field (400 mL per Minute Flow Rate)
(Coldplate with AlSiC Faceplate)

Figure 29 shows the maximum heat flux dissipated for each faceplate material choice as it varies with the coolant flow rate. All of the configurations modeled yield promising performance predictions. Given the significant performance enhancement of copper as a faceplate material, further tradeoff analysis may be considered between MMC as a faceplate material and alternative solutions to the electronics/faceplate CTE mismatch.

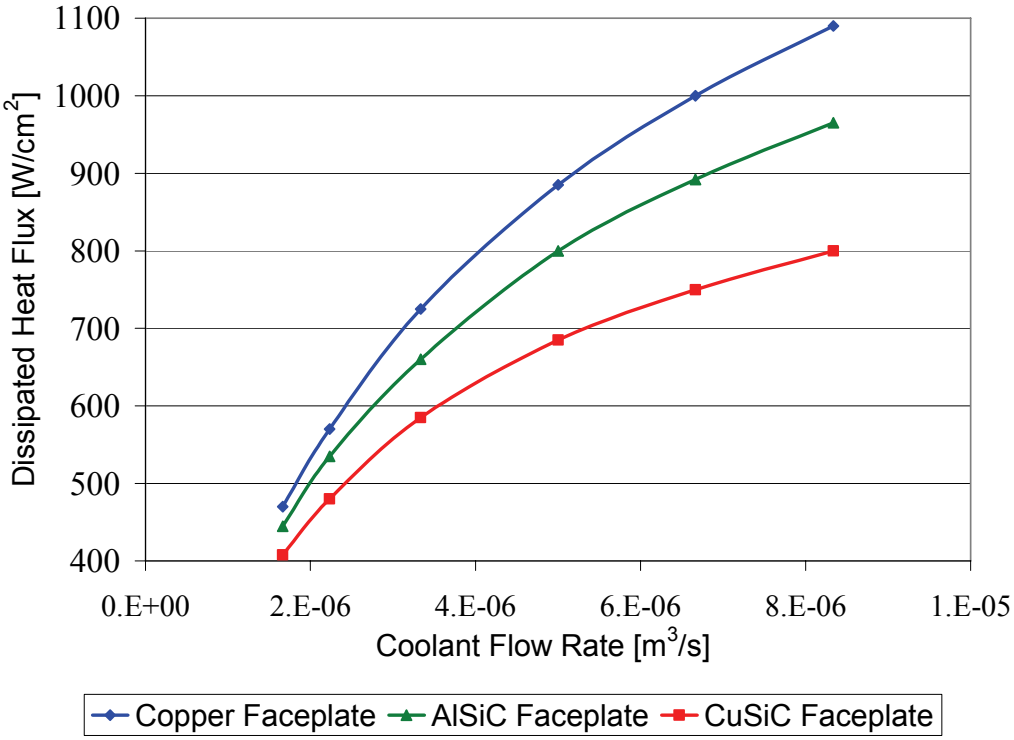

Figure 29: Faceplate Thermal Conductivity Study:
Predicted Coldplate Thermal Performance

COPPER FOAM ELEMENT EXPERIENCING COOLANT BYPASS

Prompted by unexpectedly low pressure drop measurements during initial experimental coldplate testing in May 2004, new predictive models were constructed in Fluent based off of the ligament diameter-matching models to test the hypothesis of coolant bypass around the foam element inside the coldplate as shown in Figure 30. The suspected

root cause of such a bypass was a gap between the foam and the coldplate body caused by manufacturing tolerances. Three models were constructed for the coolant flow rate of 2.0×10^{-6} m^3/s [134 mL/min], each with a different uniform gap height between the top surface of the foam element and the underside of the coldplate faceplate. Given the reasonable thermal performance of the experimental porous foam coldplate, the foam element seems to be in good contact with the faceplate in at least a portion of the foam element. This suggests that the gap may be located off-center of the streamwise symmetry axis. Such an asymmetry would permit coolant bypass without entirely breaking the conduction heat path between the faceplate and the foam element.

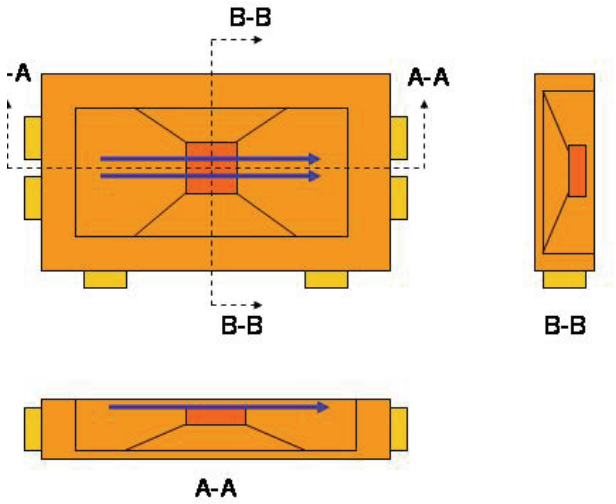

Figure 30: Diagram of Potential Root Cause of Low Coldplate Pressure Drop Experimental Results

Assuming a uniform gap height across the width of the foam element, the relationship between pressure drop across the coldplate and the gap height is depicted in Figure 31. Interpolating between models yields the estimate of a 0.26 mm gap when compared with the pressure drop measured for a coolant flow rate of 2.0×10^{-6} m^3/s [134 mL/min].

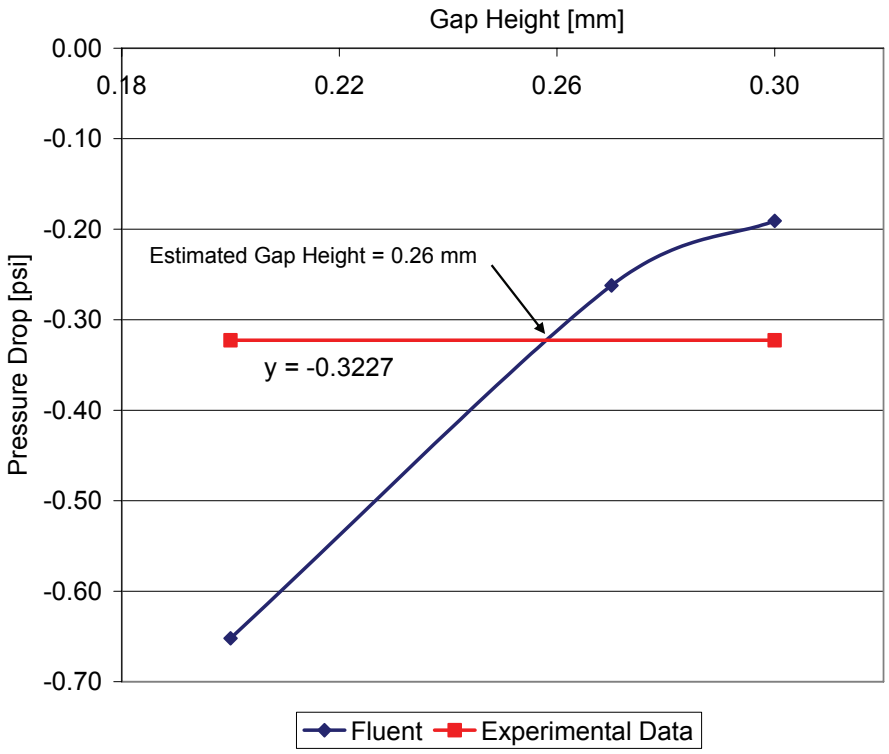

Figure 31: Total Coldplate Pressure Drop vs. Gap Height Between Faceplate and Foam (Coolant Flow Rate = 2.0×10^{-6} m^3/s [134 mL/min])

Upon the completion of the experimental characterization, the porous foam coldplate was removed from the test stand, visually examined, and photographed. As Figures 32 and 33 illustrate, a region of the faceplate had buckled. This region measured approximately 6 mm in the cross-streamwise direction, 11 mm in the streamwise direction, and 1 mm in height above the remainder of the faceplate. The buckled region was off-center of the streamwise symmetry line of the coldplate, covering only a portion of the foam element.

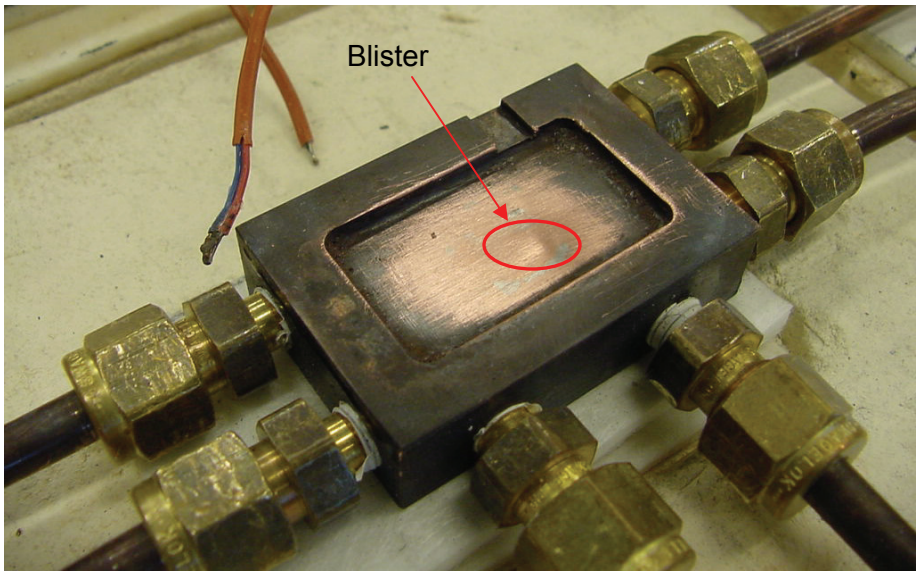

Figure 32: Coolant Bypass Blister Image 1

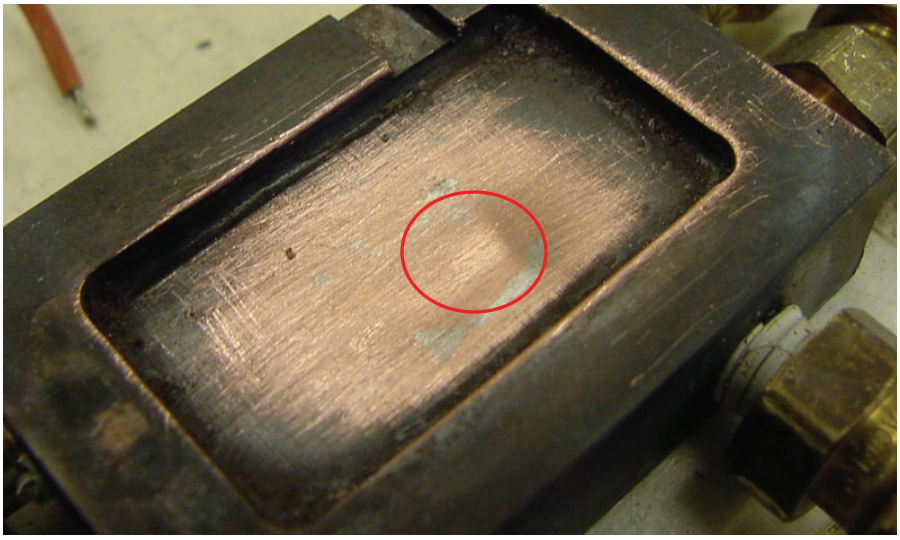

Figure 33: Coolant Bypass Blister Image 2

The porous foam coldplate was cross-sectioned for a closer view of the bypass region. Figure 34 shows the bypass region as seen from the inlet of the coldplate. The conclusion is that the coolant bypassed the foam between the top of the foam and the bottom of the faceplate where it had buckled. This substantiates the hypothesis that coolant bypass was the cause of the unexpectedly low pressure drop measurements.

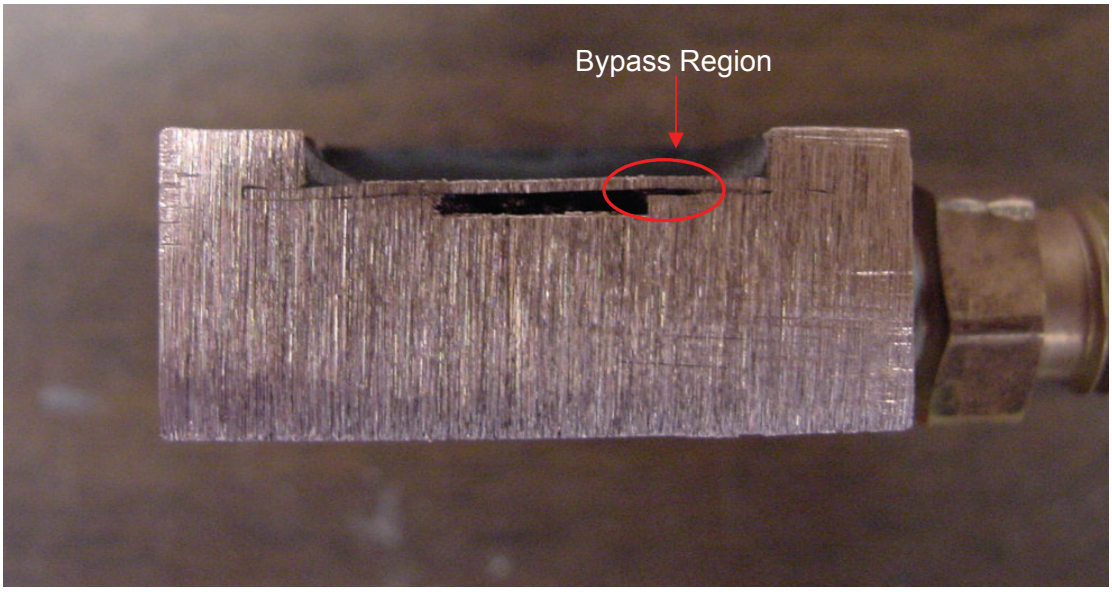

Figure 34: Porous Foam Coldplate Cross-section Image

4.2 Experimental Characterization

The coldplate experimental evaluation occurred in two stages such that for the initial coldplate design the preliminary performance results were recorded in May 2004 and more accurate final performance results were recorded in January 2005 after improvements to the test stand were completed. The preliminary results were inaccurate due to insufficient insulation of the copper tubing at the coldplate exit and of the thermocouple measuring this exit coolant temperature. Because of this, the exiting coolant was allowed to dissipate heat to the environment prior to being measured. This error caused the perceived heat input to the coolant to be smaller than it actually was.

Using fiberglass paper, the exit tubing, exit coolant-measuring thermocouple and gaps between calcium silicate pieces were insulated and filled respectively. The thermal contact resistance between the heaters and heat-focusing block was reduced by soldering the interface. The final porous copper coldplate experimental results were

recorded in January 2005 and are shown in Figures 18, 19, and 20 and Tables 5 and 6 alongside the modeling results for comparison.

UNCERTAINTY ANALYSIS OF EXPERIMENTAL DATA

During the course of the coldplate characterization, four critical measurements are taken with a known level of uncertainty due to instrumentation error. The coolant flow rate is measured with an accuracy of +/- 10.12 mL/min. The flowmeter is accurate to within +/- 2% of full-scale which is 506 mL/min. The differential pressure drop measurement is taken with an accuracy of +/- 0.016 psi, based on the ability of the data acquisition system to measure a voltage within +/- 0.00406 V. The electrical power provided to the strip heaters is measured with an accuracy of +/- 0.002 W, based on the DC power supply's following measurement accuracy: +/- 0.145 V and +/- 0.017 A. The temperature is measured using thermocouples which have been calibrated to an accuracy of +/- 1.016°C. A final source of uncertainty is the heat losses from the characterization system to the environment via natural convection and radiation. Employing a simple MATLAB code, an iterative technique was used to estimate said losses for each of the primary surfaces of the heat-focusing block. The analytical estimate of the heat losses is approximately 7.4 W for an applied heat flux of 1 kW/cm^2, a 0.74% loss.

CHAPTER 5

CONCLUSIONS

In this investigation, three periodic three-dimensional unit cells were developed to predict the thermal performance and pressure drop of porous foam coldplates for high heat flux applications such as power electronics and also to better understand the role ligament diameter, porosity, and foam effective thermal conductivity play in the construction of an accurate predictive model. In order to evaluate the accuracy of said models, a compact heat exchanger characterization test stand was designed using CFD software, constructed, and employed to test a porous foam coldplate which contained 100 ppi copper foam with 20% porosity. Comparison of multiple computational models which incorporated either orthogonal lattices of ligaments or tortuous three-dimensional pore systems with the experimental test results revealed several insights. Universal conclusions could not be made between the modeling and experimental results due to the coolant bypass which occurred within the experimental coldplates during characterization. Collectively the models predicted thermal resistances in the range of 0.07 to 0.23 °C/W for the flow and heat flux scenarios considered. The experimental characterization yielded similar thermal resistance measurements in the range of 0.09 to 0.25 °C/W despite experiencing coolant bypass. Conclusions can be drawn regarding which model prediction most closely matched the experimental results during coolant bypass. The modeling approach which most closely predicted the performance of the experimental coldplate was the ligament unit cell model which had a porosity equivalent to that of the physical microstructure of the foam under investigation. In addition, the effective thermal conductivity which couples with the porosity-matched ligament model to provide the

most accurate prediction of the performance of the experimental coldplate is 0.33 that of the foam material's thermal conductivity. This result is similar to that of Evans who reported a scaling factor of 0.28 for ERG foam material. The conclusions of this investigation are not universal for all porous foam coldplates but can be applied to those with coolant bypass such as the coldplate evaluated in this investigation.

CHAPTER 6

RECOMMENDATIONS

Recommended future work includes the construction and experimental evaluation of porous copper coldplates which do not experience coolant bypass, the evaluation of coldplates filled with alternative material foams such as graphite, and the determination of the accuracy of the unit cell open ligament modeling technique for such thermal management foam materials. Size reduction of the characterization hardware would also be a worthwhile future work.

APPENDIX A

PUBLISHED WORK

S. Wilson, Y. Joshi, B. Rozenoyer, and U. Kashalikar, “Investigation of Copper Foam Coldplates as a High Heat Flux Electronics Cooling Solution,” *Proceedings of the 10th International Workshop on Thermal Investigations of ICs and Systems (THERMINIC)*, Sophia Antipolis, France, 213-216, Sept. 29-Oct. 1, 2004.

REFERENCES

[1] Philip E. Ross, “Beat the Heat,” *IEEE Spectrum*, pp. 38-43, May 2004.

[2] Alain Bricard and Christian Schaeffer, “The Problem of Electronics Cooling, and Solutions,” *CLEFS CEA,* No. 44, pp. 94-96, 2000.

[3] J.A. Herbsommer, H. Safar, W. Brown, E.W. Lau, D.P. Farrell, P. Gammel, O. Lopez, and G. Terefenko, “Improved Electrical and Thermal Performance of Ultrathin RF LDMOS Power Transistors,” Agere Systems Inc. White Paper, 2003.

[4] S. Seshadri, W.B. Hall, J.C. Kotvas, and P.A. Sanger, “100kHz Operation of SiC Junction Controlled Thyristor (JCT) Switches used in an All-SiC PWM Inverter,” *Materials Science Forum*, Vol. 338, pp. 1403-1406, 2000.

[5] D. Mundinger, R. Beach, W. Benett, R. Solarz, W. Krupke, R. Staver, and D. Tuckerman, “Demonstration of High-Performance Silicon Microchannel Heat Exchangers for Laser Diode Array Cooling,” *Applied Physics Letters*, Vol. 53, No. 12, pp. 1030-1032, 1988.

[6] G.L. Harnagel, P.S. Cross, C.R. Lennon, M. Devito, and D.R. Scifres, “Ultra-High-Power Quasi-CW Monolithic Laser Diode Arrays with High Power Conversion Efficiency,” *Electronic Letters*, Vol. 23, No. 14, pp. 743-744, 1987.

[7] V.V. Apollonov, A.I. Barchukov, V.I. Borodin, P.I. Bystrov, V.F. Goncharov, L.M. Ostrovskaya, A.M. Prokhorov, V.N. Rodin, E.V. Trushin, V. Yu. Khomich, M.I. Tsypin, Yu. F. Shevakin, and Ya. Sh. Shur, “Possibility of Using Structures with Open Pores in Construction of Cooled Laser Mirrors,” *Soviet Journal of Quantum Electronics*, Vol. 8, No. 5, pp. 672-673, 1978.

[8] V.V. Apollonov, P.I. Bystrov, V.F. Goncharov, A.M. Prokhorov, and V. Yu. Khomich, “Prospects for the Use of Porous Structures for Cooling Power Optics Components,” *Soviet Journal of Quantum Electronics*, Vol. 9, No. 12, pp. 1499-1505, 1979.

[9] V.V. Apollonov, P.I. Bystrov, S.A. Chyotkin, V.G. Goncharov, V. Yu. Khomich, and A.M. Prokhorov, “The Promising Use of Some Heat Carriers in High Intensity Laser Optics,” *Proc. Symp. Laser Induced Damage in Optical Materials*, pp. 328-338, 1980.

[10] V.E. Zapevalov, A.P. Keyer, V.E. Myosknikov, S.A. Madiegan, and V.A. Flyagin, “Development of High-Powered Gyrotrons at 140 GHz,” *Microwave Tube Journal* (In Russian), 1991.

[11] J.H. Rosenfeld, R. Schumacher, R.D. Watson, and J.M. McDonald, “Test Results from a Pumped Single Phase Porous Metal Heat Exchanger,” *High Heat Flux Engineering II,* Vol. 1997, pp. 53-64, 1993.

[12] M.T. North, J.H. Rosenfeld, and D.L. Youchison, “Test Results from a Helium Gas-Cooled Porous Metal Heat Exchanger,” *High Heat Flux Engineering III,* Vol. 2855, pp. 54-65, 1996.

[13] J.H. Rosenfeld and M.T. North, “Porous Media Heat Exchangers for Cooling of High-Power Optical Components,” *Optical Engineering*, Vol. 34, No. 2, pp. 335-341, 1995.

[14] V.V. Apollonov, S.I. Derzhavin, V.V. Kuzminov, D.A. Mashkovskiy, V.N. Timoshkin, and V.A. Philonenko, “Intensification of Heat Transfer in High-Power Laser Diode Bars by Means of a Porous Metal Heat-Sink,” *Optics Express*, Vol. 4, No. 1, pp. 27-32, 1999.

[15] V.V. Apollonov, S.I. Derzhavin, V.A. Filonenko, V.V. Kuzminov, D.A. Mashkovsky, A.M. Prokhorov, and V.N. Timoshkin, “Highly Efficient Heat Exchangers for Laser Diode Arrays,” *Advanced High-Power Lasers*, Vol. 3889, pp. 71-81, 2000.

[16] H. Darcy, *Les Fontaines Publiques de la ville de Dijon*, Dalmont, Paris, 1856.

[17] H. Brenner, “Dispersion Resulting from Flow through Spatially Periodic Porous Media,” *Phil. Trans. of the Royal Soc. of London. Series A*, Vol. 297, No. 1430, pp. 81-133, 1980.

[18] D.L. Koch, R.G. Cox, H. Brenner, and J.F. Brady, “The Effect of Order on Dispersion in Porous Media,” *Journal of Fluid Mechanics*, Vol. 200, pp. 173-188, 1989.

[19] A.-F. Bastawros and A.G. Evans, “Characterization of Open-Cell Aluminum Alloy Foams As Heat Sinks for High Power Electronic Devices,” *ASME EEP-Vol. 23/HTD-Vol. 356, CAE/CAD and Thermal Management Issues in Electronic Systems*, pp. 1-6, 1997.

[20] T.J. Lu, H.A. Stone, and M.F. Ashby, “Heat Transfer in Open-Cell Metal Foams,” *Acta Materialia*, Elsevier Science Ltd., Great Britain, Vol. 46, No. 10, pp. 3619-3635, 1998.

[21] K. Boomsma and D. Poulikakos, “On the Effective Thermal Conductivity of a Three-Dimensionally Structured Fluid-Saturated Metal Foam,” *International Journal of Heat and Mass Transfer,* Vol. 44, pp. 827-836, 2001.

[22] K. Boomsma, D. Poulikakos, and Y. Ventikos, “Simulations of Flow Through Open Cell Metal Foams Using an Idealized Periodic Cell Structure,” *International Journal of Heat and Fluid Flow*, Vol. 24, pp. 825-834, 2003.

[23] *Fluent 6 User’s Guide*, Fluent Inc., Lebanon, NH, 2001.

[24] Kambiz Vafai (editor), *Handbook of Porous Media*, Marcel Dekker, Inc., New York, 2000.

[25] M. Kaviany, *Principles of Heat Transfer in Porous Media*, Springer-Verlag, New York, 1991.

[26] V.V. Kharitonov, A.A. Plakseev, V.N. Fedoseev, and V.V. Voskoboinikov, “Effect of Fluid Mixing on Heat Transfer in Channels with Porous Inserts,” *Teplofizika Vysokikh Temperatur,* Vol. 25, No. 5, pp. 954-961, 1987.

[27] A.G. Evans, J.W. Hutchinson, and M.F. Ashby, “Cellular Metals,” *Current Opinions in Solid State & Materials Science,* Vol. 3, pp. 288-303, 1998.